nature immunology

The ion channel TRPV1 regulates the activation and proinflammatory properties of CD4+ T cells

Samuel Bertin[1], Yukari Aoki-Nonaka[1,2], Petrus Rudolf de Jong[1], Lilian L Nohara[3,8], Hongjian Xu[3,8], Shawna R Stanwood[3], Sonal Srikanth[4], Jihyung Lee[1], Keith To[1], Lior Abramson[1], Timothy Yu[1], Tiffany Han[1], Ranim Touma[5], Xiangli Li[1], José M González-Navajas[1], Scott Herdman[1], Maripat Corr[1], Guo Fu[6,7], Hui Dong[1], Yousang Gwack[4], Alessandra Franco[5], Wilfred A Jefferies[3] & Eyal Raz[1]

TRPV1 is a Ca^{2+}-permeable channel studied mostly as a pain receptor in sensory neurons. However, its role in other cell types is poorly understood. Here we found that TRPV1 was functionally expressed in $CD4^+$ T cells, where it acted as a non–store-operated Ca^{2+} channel and contributed to T cell antigen receptor (TCR)-induced Ca^{2+} influx, TCR signaling and T cell activation. In models of T cell–mediated colitis, TRPV1 promoted colitogenic T cell responses and intestinal inflammation. Furthermore, genetic and pharmacological inhibition of TRPV1 in human $CD4^+$ T cells recapitulated the phenotype of mouse *Trpv1*$^{-/-}$ $CD4^+$ T cells. Our findings suggest that inhibition of TRPV1 could represent a new therapeutic strategy for restraining proinflammatory T cell responses.

© 2014 Nature America, Inc. All rights reserved.

Following engagement of the T cell antigen receptor (TCR) and formation of the immunological synapse, calcium (Ca^{2+}) channels mediate the Ca^{2+} influx necessary for the activation of T cells[1]. Ca^{2+} influx from the extracellular milieu into the cytosol is mandatory for the activation of downstream TCR signaling pathways and key transcription factors, including NFAT and NF-κB[2]. Ligation of the TCR triggers phosphorylation events that lead to activation of the Ca^{2+} release–activated Ca^{2+} channel complex and to store-operated Ca^{2+} entry[3]. However, this canonical scheme of Ca^{2+} influx does not account for the involvement of other plasma-membrane Ca^{2+} channels.

Studies have documented the important contributions of voltage-gated Ca^{2+} channels[4,5] and members of the transient receptor potential (TRP) family of ion channels[6,7] to T cell activation. The mammalian TRP family of ion channels consists of 28 members categorized into six subfamilies: canonical (TRPC), with seven members; vanilloid (TRPV), with six members; melastatin (TRPM), with eight members; ankyrin (TRPA), with one member; polycystin (TRPP), with three members; and mucolipin (TRPML), with two members[8]. Although physiological roles of TRP channels are well characterized in the nervous system, their role in the activation and function of T cells is still elusive[2,5,6].

The 'founding member' of the TRPV subfamily, TRPV1, is highly permeable to Ca^{2+} (with a permeability to calcium relative to permeability to sodium (P_{Ca}/P_{Na}) of ~10)[9] and was initially identified as the receptor for capsaicin, the pungent ingredient in chili peppers[10]. In this study, we found that mouse and human primary $CD4^+$ T cells expressed a functional TRPV1 channel (called '$TRPV1^{CD4}$' here). We found that $TRPV1^{CD4}$ contributed to TCR-induced Ca^{2+} influx and was required for proper downstream TCR signaling. Our data indicate a cell-intrinsic role for the TRPV1 channel in the activation of and acquisition of proinflammatory properties by $CD4^+$ T cells.

RESULTS

Expression of functional TRPV1 by $CD4^+$ T cells

We first compared the expression of mRNA encoding various TRP channels in primary $CD4^+$ T cells isolated from the spleen of C57BL/6 (wild-type) mice. Among mRNA encoding the eight different TRP channels analyzed, *Trpv1* transcripts had the highest expression (**Fig. 1a**). We used $CD4^+$ T cells isolated from *Trpv1*$^{-/-}$ mice as a control (**Fig. 1b**). We confirmed expression of TRPV1 protein in mouse spleen $CD4^+$ T cells by flow cytometry (**Fig. 1c**) as well as in human primary $CD4^+$ T cells and in the Jurkat human T lymphocyte cell line by immunoblot analysis (**Supplementary Fig. 1a**). Confocal microscopy showed expression of TRPV1 predominantly at the plasma membrane of resting $CD4^+$ T cells (**Fig. 1d** and **Supplementary Fig. 1b**,**c**). Indeed, the fluorescence signals of TRPV1 and CD4 were largely colocalized (Pearson's correlation coefficient, 0.96) (**Fig. 1e**). Furthermore, cell-surface biotinylation assays confirmed localization of TRPV1 at the plasma membrane of Jurkat T cells (**Supplementary Fig. 1d**).

We next evaluated the functionality of the TRPV1 channel in $CD4^+$ T cells by the whole-cell patch-clamp technique. We used the prototypical TRPV1 agonist capsaicin[10] and recorded capsaicin-induced

[1]Department of Medicine, University of California, San Diego, La Jolla, California, USA. [2]Division of Oral Science for Health Promotion, Niigata University Graduate School of Medical and Dental Sciences, Niigata, Japan. [3]Michael Smith Laboratories, Centre for Blood Research, The Brain Research Centre, Department of Medical Genetics, Department of Microbiology and Immunology and Department of Zoology, University of British Columbia, Vancouver, Canada. [4]Department of Physiology, David Geffen School of Medicine at University of California, Los Angeles, Los Angeles, California, USA. [5]Department of Pediatrics University of California, San Diego, La Jolla, California, USA. [6]Department of Immunology and Microbial Science, The Scripps Research Institute, La Jolla, California, USA. [7]State Key Laboratory of Cellular Stress Biology, Innovation Center for Cell Biology, School of Life Sciences, Xiamen University, Fujian, China. [8]These authors contributed equally to this work. Correspondence should be addressed to W.A.J. (wilf@msl.ubc.ca) or E.R. (eraz@ucsd.edu).

Received 28 August; accepted 11 September; published online 5 October 2014; doi:10.1038/ni.3009

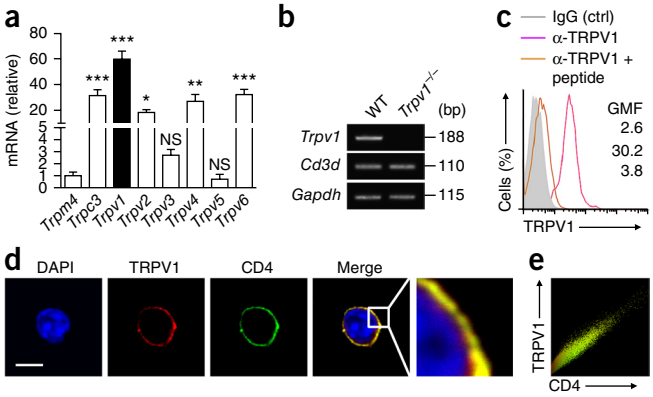

Figure 1 TRPV1 is expressed in CD4$^+$ T cells. (**a**) Quantitative PCR analysis of transcripts encoding TRP proteins in splenic CD4$^+$ T cells isolated from C57BL/6 (wild-type) mice; results normalized to those for the housekeeping gene *Gapdh* (encoding GAPDH) and presented relative to those for *Trpm4* (known to be expressed in CD4$^+$ T cells[27]), set as 1. NS, not significant; $*P < 0.05$, $**P < 0.001$ and $***P < 0.0001$ (one-way analysis of variance (ANOVA) with post-hoc Dunnett's test). (**b**) Electrophoresis of the products of quantitative PCR analysis of splenic CD4$^+$TCRβ$^+$ T cells isolated from wild-type (WT) and *Trpv1*$^{-/-}$ mice and sorted by flow cytometry (purity, >98%): the *Trpv1*-specific product (top) migrates at the expected size of 188 base pairs (bp); *Cd3d* (encoding CD3δ) serves as a T cell marker; *Gapdh* (encoding glyceraldehyde phosphate dehydrogenase) serves as a loading control. (**c**) Flow cytometry of splenocytes isolated from wild-type mice, preincubated with a blocking peptide corresponding to TRPV1 (α-TRPV1 + peptide) or not (α-TRPV1) and then stained for CD4 and TCRβ (gated as CD4$^+$TCRβ$^+$ T cells) and with anti-TRPV1, or stained with the isotype-matched control antibody immunoglobulin G alone (IgG) (ctrl); numbers in plot indicate geometric mean fluorescence (GMF) of the staining intensity. (**d**) Confocal microscopy of the subcellular localization of TRPV1 and CD4 in splenic CD4$^+$ T cells stained with the DNA-binding dye DAPI (far left), with goat anti-TRPV1 (primary) followed by Alexa Fluor 546–conjugated anti-goat (secondary) (middle left) or with Alexa Fluor 488–conjugated anti-CD4 (middle); middle right, merged image (yellow, TRPV1-CD4 colocalization); far right, enlargement (5.5×) of area outlined at left. Scale bar, 5 μm. (**e**) Colocalization of TRPV1 and CD4, assessed with Velocity software (Pearson's correlation coefficient, 0.96). Data are representative of three or more independent experiments (mean and s.e.m. of five mice in **a**).

© 2014 Nature America, Inc. All rights reserved.

currents in wild-type and *Trpv1*$^{-/-}$ CD4$^+$ T cells held at –85 mV (**Fig. 2a**). In wild-type CD4$^+$ T cells, the application of capsaicin rapidly induced a small inward current (1.7 ± 0.4 pA/pF (mean ± s.e.m.); $n = 9$ cells) that was desensitized with prolonged exposure to the agonist (**Fig. 2a**,**b**). This desensitization was probably caused by the presence of Ca^{2+} ions in the external solution, as demonstrated before in recordings of rat TRPV1 currents in HEK293 human embryonic kidney cells transfected to express TRPV1 (refs. 10,11). In *Trpv1*$^{-/-}$ CD4$^+$ T cells, we recorded only an insignificant amount of inward current (0.4 ± 0.1 pA/pF (mean ± s.e.m.); $n = 8$ cells) in response to capsaicin (**Fig. 2a**,**b**). Additionally, with the same recording conditions, we routinely recorded 2- to 10-nA capsaicin-gated currents from transformed human kidney (tSA201) cells with transient expression of rat TRPV1 (data not shown). To further confirm that the current observed in wild-type CD4$^+$ T cells was indeed a TRPV1 current, we measured capsaicin-induced currents in the presence of SB366791, a specific TRPV1 antagonist[12]. SB366791 inhibited approximately 80% of the inward current observed in wild-type CD4$^+$ T cells in response to capsaicin (untreated control, 2.0 ± 0.3 pA/pF (mean ± s.e.m.), $n = 10$ cells; SB366791 treated, 0.4 ± 0.1 pA/pF (mean ± s.e.m.), $n = 13$ cells) (**Fig. 2a**,**c**). To better characterize the capsaicin-induced current in CD4$^+$ T cells, we used a ramp-pulse protocol to measure the current-voltage relationship after the addition of capsaicin (**Fig. 2d**). The current-voltage relationship of the capsaicin-gated current confirmed the outward-rectification characteristic of the TRPV1 current reported for rat and human TRPV1 channels[10,12].

To further evaluate functionality of the TRPV1 channel in CD4$^+$ T cells, we performed single-cell ratiometric Ca^{2+} imaging and flow

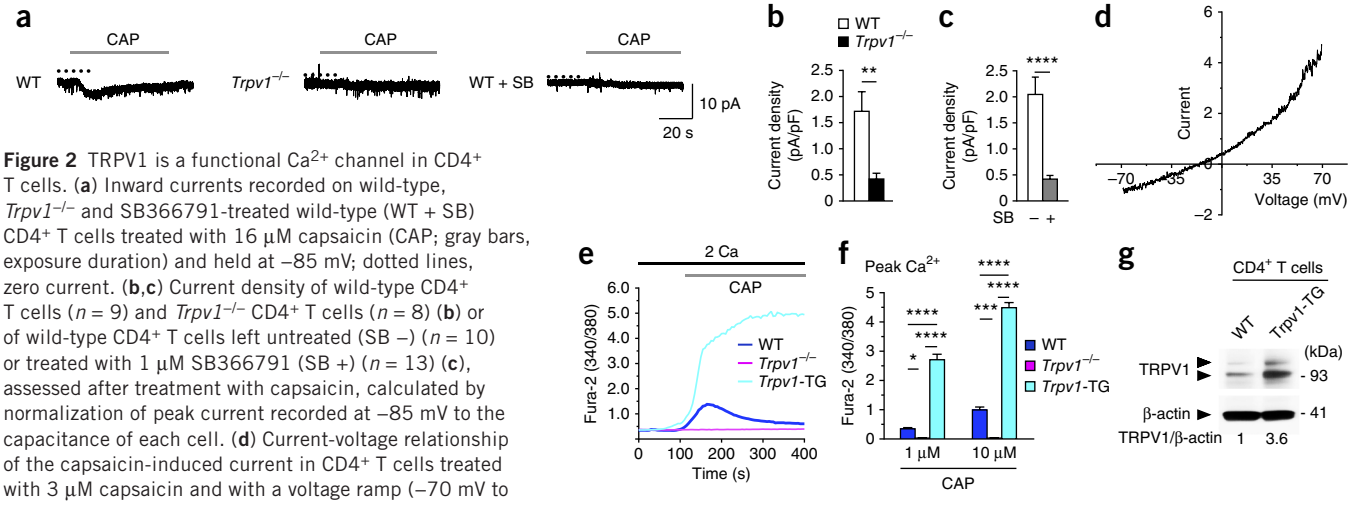

Figure 2 TRPV1 is a functional Ca^{2+} channel in CD4$^+$ T cells. (**a**) Inward currents recorded on wild-type, *Trpv1*$^{-/-}$ and SB366791-treated wild-type (WT + SB) CD4$^+$ T cells treated with 16 μM capsaicin (CAP; gray bars, exposure duration) and held at –85 mV; dotted lines, zero current. (**b**,**c**) Current density of wild-type CD4$^+$ T cells ($n = 9$) and *Trpv1*$^{-/-}$ CD4$^+$ T cells ($n = 8$) (**b**) or of wild-type CD4$^+$ T cells left untreated (SB –) ($n = 10$) or treated with 1 μM SB366791 (SB +) ($n = 13$) (**c**), assessed after treatment with capsaicin, calculated by normalization of peak current recorded at –85 mV to the capacitance of each cell. (**d**) Current-voltage relationship of the capsaicin-induced current in CD4$^+$ T cells treated with 3 μM capsaicin and with a voltage ramp (–70 mV to +70 mV) delivered over 400 ms; results calculated by subtraction of current before the addition of capsaicin from current after that addition and normalization relative to the current at –70 mV (–19.2 ± 3.3 pA). (**e**) $[Ca^{2+}]_i$ in wild-type, *Trpv1*$^{-/-}$ and *Trpv1*-TG splenic CD4$^+$CD25$^-$ (naive) T cells loaded with the calcium indicator Fura-2 AM and treated with 10 μM capsaicin (gray bar) in the presence of 2 mM $CaCl_2$ (2 Ca; black bar), monitored by confocal imaging and presented as the ratio of Fura-2 emission at an excitation of 340 nm to that at 380 nm (340/380). (**f**) Quantification of Ca^{2+}-influx profiles obtained as in **e** with 1 or 10 μM capsaicin. (**g**) Immunoblot analysis of TRPV1 and β-actin (loading control throughout) in total lysates of wild-type and *Trpv1*-TG splenic CD4$^+$ T cells; doublets at ~95 kilodaltons (kDa) and 115 kDa correspond to the nonglycosylated and glycosylated forms of the TRPV1 channel[40]. Below lanes, densitometry analysis (band intensity relative to that of β-actin). $*P < 0.05$, $**P < 0.01$, $***P < 0.001$ and $****P < 0.0001$ (two-tailed Student *t*-test (**b**,**c**) or one-way ANOVA with the *post-hoc* Bonferroni test (**f**)). Data are representative of three or more independent experiments (mean and s.e.m. in **b**,**c**; average of four cells in **d**; mean and s.e.m. of 50–100 cells in **f**).

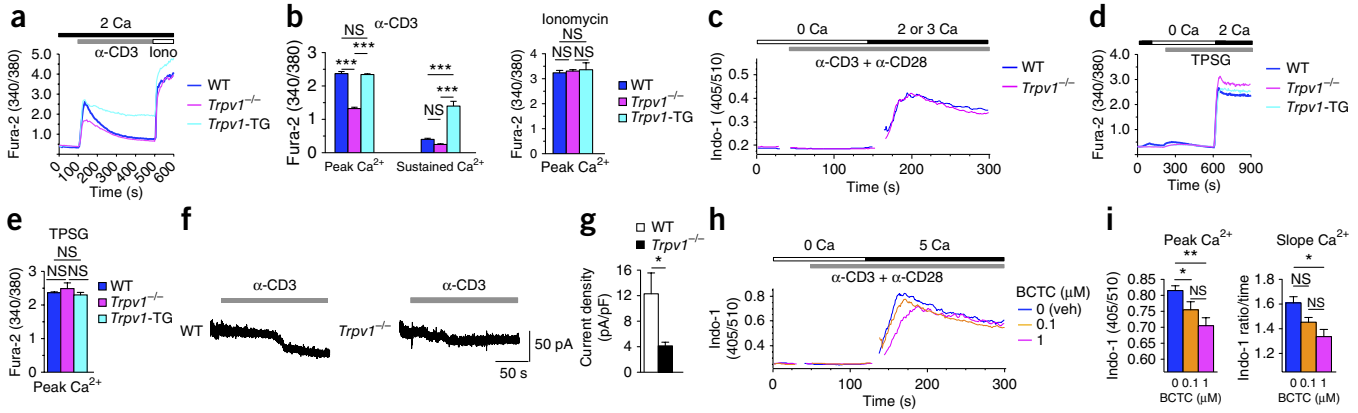

Figure 3 TRPV1^{CD4} acts as a non–store-operated Ca^{2+} channel and contributes to TCR-induced Ca^{2+} influx. (**a**) $[Ca^{2+}]_i$ in wild-type, *Trpv1*$^{-/-}$ and *Trpv1*-TG splenic CD4$^+$CD25$^-$ (naive) T cells loaded with Fura-2 AM and stimulated by crosslinking with anti-CD3 (α-CD3) in the presence of 2 mM $CaCl_2$ (2 Ca), with 1 μM ionomycin (Iono) added at the end of the acquisition (monitored and presented as in **Fig. 2e**). (**b**) Quantification of the Ca^{2+}-influx profiles in **a**. (**c**) $[Ca^{2+}]_i$ in wild-type and *Trpv1*$^{-/-}$ spleen CD4$^+$ T cells loaded with the fluorescent Ca^{2+} indicator dye Indo-1 AM and stimulated with soluble anti-CD3 (10 μg/ml) and anti-CD28 (1 μg/ml) (α-CD3 + α-CD28) in Ca^{2+}-free medium, assessed before (0 Ca) and after (2 or 3 Ca) the addition of $CaCl_2$ (2 mM (wild-type) or 3 mM (*Trpv1*$^{-/-}$)) to the extracellular medium, monitored by flow cytometry; results are presented as the ratio of Indo-1 emission at 405 nm to that at 510 nm (405/510). (**d**) Store-operated Ca^{2+} entry in wild-type, *Trpv1*$^{-/-}$ and *Trpv1*-TG splenic CD4$^+$CD25$^-$ (naive) T cells loaded with Fura-2 AM, assessed before (0 Ca) and after (2 Ca) the addition of 2 mM $CaCl_2$ and after passive depletion of intracellular stores with 1 μM thapsigargin (TPSG). (**e**) Quantification of the Ca^{2+}-influx profiles in **d**. (**f**) Inward currents in wild-type and *Trpv1*$^{-/-}$ CD4$^+$ T cells activated by crosslinking with anti-CD3 and streptavidin (bar above also indicates duration of streptavidin application), and held at −85 mV. (**g**) TCR-induced currents in wild-type CD4$^+$ T cells ($n = 7$) and *Trpv1*$^{-/-}$ CD4$^+$ T cells ($n = 9$), calculated by normalization of peak current to capacitance of each cell. (**h**) $[Ca^{2+}]_i$ in wild-type CD4$^+$ T cells loaded with Indo-1 AM and pretreated for 5 min with the TRPV1 antagonist BCTC (0.1 or 1 μM) or vehicle alone (veh; 0.1% dimethyl sulfoxide (DMSO)), then stimulated with anti-CD3 plus anti-CD28 in Ca^{2+}-free medium, with 5 mM $CaCl_2$ (5 Ca) added to the extracellular medium during the acquisition (presented as in **c**). (**i**) Quantification of the Ca^{2+}-influx profiles in **h**. $^*P < 0.05$; $^{**}P < 0.01$ and $^{***}P < 0.0001$ (two-tailed Student *t*-test (**g**) or one-way ANOVA with the *post-hoc* Bonferroni test (**b**,**e**,**i**)). Data are representative of three or more independent experiments (mean and s.e.m. of 50–100 cells in **b**,**e**; mean and s.e.m. in **g**,**i**).

cytometry–based Ca^{2+} flux measurements. Capsaicin increased the intracellular calcium concentration ($[Ca^{2+}]_i$) in a concentration-dependent way in wild-type naive CD4$^+$ T cells but not in their *Trpv1*$^{-/-}$ counterparts (**Fig. 2e**,**f**). In addition, we generated mice with transgenic expression of TRPV1 specifically in CD4$^+$ T cells (*Trpv1*-TG mice) by crossing mice expressing *Trpv1* from the ubiquitous *Rosa26* locus[13] with mice expressing Cre recombinase from the T cell–specific *Cd4* promoter. We found that capsaicin induced a substantial Ca^{2+} influx in *Trpv1*-TG CD4$^+$ T cells (**Fig. 2e**,**f**) that overexpressed TRPV1 (**Fig. 2g**). Capsaicin also induced a substantial Ca^{2+} influx in Jurkat T cells, which was almost completely abolished after knockdown of TRPV1 mediated by short hairpin RNA (**Supplementary Fig. 1e**). Collectively, these findings indicated that the TRPV1 channel was functionally expressed on the plasma membrane of CD4$^+$ T cells (TRPV1^{CD4}).

TRPV1^{CD4} contributes to TCR-induced Ca^{2+} influx

We next investigated the physiological role of TRPV1^{CD4} by comparing changes in $[Ca^{2+}]_i$ after stimulation of the TCR in wild-type, *Trpv1*$^{-/-}$ and *Trpv1*-TG CD4$^+$ T cells. Ca^{2+} influx induced by crosslinking with antibody to the invariant signaling protein CD3 (anti-CD3) was significantly lower in *Trpv1*$^{-/-}$ CD4$^+$ T cells than in wild-type cells (**Fig. 3a**,**b**). We observed this defect in *Trpv1*$^{-/-}$ CD4$^+$ T cells independently of the extracellular calcium concentration tested or of the Ca^{2+} flux–monitoring protocol used (for example, TCR stimulation before the addition of $CaCl_2$ or vice versa; **Supplementary Fig. 2a–d**). In addition, Ca^{2+}-titration experiments revealed that the TCR-induced Ca^{2+} influx defect in *Trpv1*$^{-/-}$ CD4$^+$ T cells was 'rescued' by a 50% increase in the extracellular calcium concentration in the culture medium (**Fig. 3c**). In accordance with the localization of TRPV1^{CD4} at the plasma membrane (**Fig. 1d**,**e** and **Supplementary Fig. 1d**), the Ca^{2+} efflux from intracellular stores was similar in wild-type and *Trpv1*$^{-/-}$ CD4$^+$ T cells after stimulation of the TCR (**Supplementary Fig. 2e**). The TCR-induced Ca^{2+} influx was significantly more sustained in *Trpv1*-TG CD4$^+$ T cells than in wild-type cells (**Fig. 3a**,**b** and **Supplementary Fig. 2f**). However, we observed no difference among wild-type, *Trpv1*$^{-/-}$ and *Trpv1*-TG CD4$^+$ T cells in Ca^{2+} influx following stimulation with the Ca^{2+} ionophore ionomycin (**Fig. 3a**,**b** and **Supplementary Fig. 2g**,**h**) or with the sarcoplasmic reticulum Ca^{2+}-ATPase pump inhibitor thapsigargin (**Fig. 3d**,**e** and **Supplementary Fig. 2i**), which bypass proximal TCR signaling and induce activation of Ca^{2+} release–activated Ca^{2+} channels and store-operated Ca^{2+} entry[14]. Since TRPV3 shares 40–50% homology with TRPV1 and can form heteromultimers with that channel[9,15], we also analyzed the Ca^{2+}-influx profile of spleen CD4$^+$ T cells isolated from *Trpv3*$^{-/-}$ mice. However, in contrast to Ca^{2+} influx in *Trpv1*$^{-/-}$ CD4$^+$ T cells, we found normal Ca^{2+} influx in these cells upon stimulation of the TCR (**Supplementary Fig. 2j**). We further confirmed the specific contribution of TRPV1 to TCR-induced Ca^{2+} currents by whole-cell patch-clamp experiments. Crosslinking of TCRs produced significantly smaller inward currents in *Trpv1*$^{-/-}$ CD4$^+$ T cells held at −85 mV (4.1 ± 0.6 pA/pF (mean ± s.e.m.); $n = 9$ cells) than in wild-type cells under the same experimental conditions (12.3 ± 3.3 pA/pF (mean ± s.e.m.), $n = 7$ cells) (**Fig. 3f**,**g**). Finally, pretreatment of wild-type CD4$^+$ T cells with either of two different TRPV1 antagonists, BCTC[16] (**Fig. 3h**,**i**) or I-RTX[17] (**Supplementary Fig. 2k**), decreased the Ca^{2+} influx induced by TCR stimulation to a level similar to that in *Trpv1*$^{-/-}$ CD4$^+$ T cells and did so in a concentration-dependent way. Collectively, these results suggested that TRPV1^{CD4} acted as a non–store-operated Ca^{2+} channel and contributed to TCR-induced Ca^{2+} influx.

© 2014 Nature America, Inc. All rights reserved.

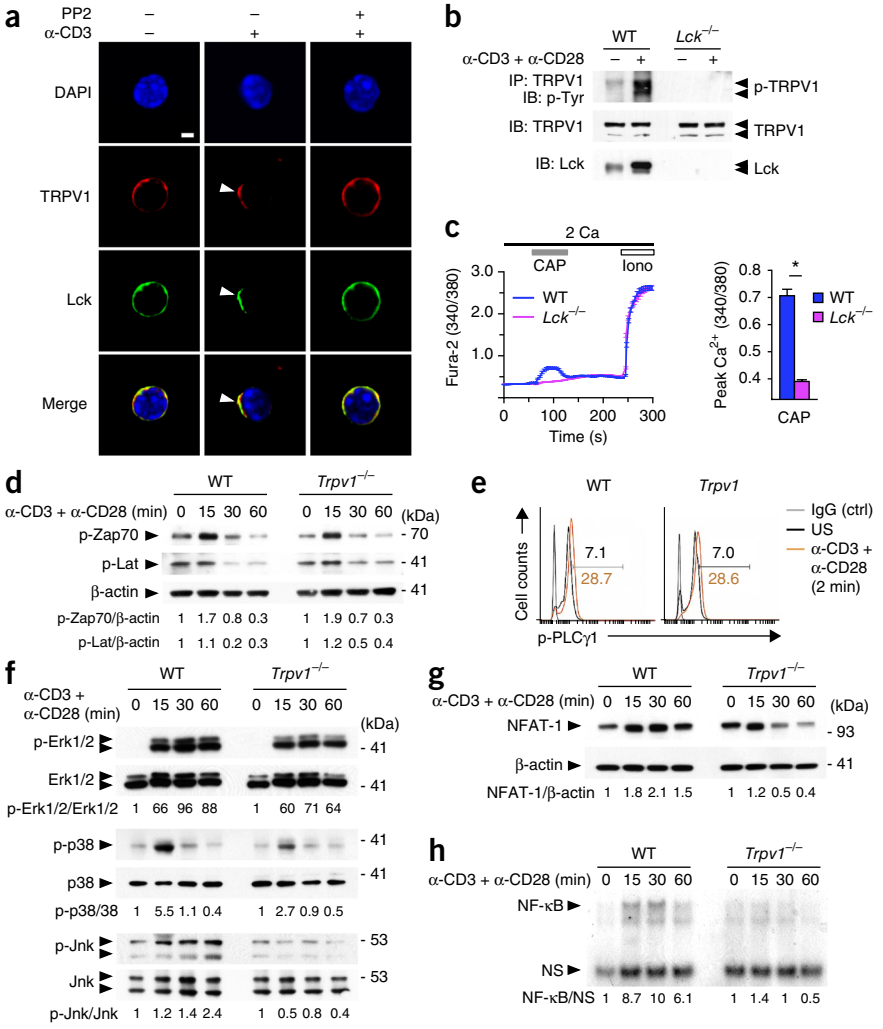

Figure 4 TRPV1^{CD4} participates in TCR signaling. (**a**) Confocal microscopy of wild-type spleen CD4$^+$ T cells before (α-CD3 –) and after (α-CD3 +) crosslinking with anti-CD3, in the presence (+) or absence (–) of the Src-family kinase inhibitor PP2 (10 μM); arrowheads indicate recruitment of TRPV1 to TCR clusters; yellow (merged images) indicates clustering of Lck and TRPV1. Scale bar, 2 μm. (**b**) Immunoassay of Jurkat E6.1 cells (wild-type) and J.CaM1.6 cells (*Lck*$^{-/-}$) left unstimulated (–) or stimulated (+) for 5 min with soluble antibody to human CD3 (2.5 μg/ml) and antibody to human CD28 (1 μg/ml), followed by immunoprecipitation (IP) with anti-TRPV1 and immunoblot analysis (IB) of immunoprecipitates (top blot) or total cell lysates (middle and bottom blots) with antibody to phosphorylated tyrosine (p-Tyr), anti-TRPV1 and anti-Lck (left margin). (**c**) $[Ca^{2+}]_i$ in wild-type and *Lck*$^{-/-}$ Jurkat T cells loaded with Fura-2 AM and treated with 1 μM capsaicin in the presence of 2 mM $CaCl_2$ (2 Ca), with the addition of 1 μM ionomycin (Iono) at the end of the acquisition (positive control) (monitored and presented as in **Fig. 2e**). Right, quantification of Ca^{2+}-influx peak at left. $^*P < 0.0001$ (two-tailed Student *t*-test). (**d**) Immunoblot analysis of phosphorylated (p-) Zap70 and Lat in the cytosolic fraction of wild-type and *Trpv1*$^{-/-}$ spleen CD4$^+$ T cells left unstimulated (0) or stimulated for 15–60 min (above lanes) with soluble anti-CD3 (5 μg/ml) and anti-CD28 (2 μg/ml). Right margin, molecular size (in kDa). (**e**) Intracellular staining of phosphorylated PLC-γ1 in gated CD4$^+$TCRβ$^+$ wild-type and *Trpv1*$^{-/-}$ splenic CD4$^+$ T cells left unstimulated (US) or stimulated for 2 min with soluble anti-CD3 (5 μg/ml) and anti-CD28 (2 μg/ml). Numbers above and below bracketed lines indicate percent PLC-γ1$^+$ cells (colors match key). (**f**) Immunoblot analysis of phosphorylated and total Erk1/2, p38 and Jnk in the cytosolic fraction of cells stimulated as in **d**. (**g**) Immunoblot analysis of NFAT-1 in the nuclear fraction of cells stimulated as in **d**. (**h**) Electrophoretic mobility-shift assay of NF-κB in the nuclear fraction of cells stimulated as in **d**; NS, nonspecific low-molecular weight band (loading control). Below lanes (**d**,**f**–**h**), densitometry analysis. Data are representative of three or more independent experiments (mean and s.e.m. of 50 cells in **c**).

TRPV1^{CD4} is part of the TCR signaling cascade

We then investigated how TRPV1^{CD4} was activated upon stimulation of the TCR and assessed its effect on TCR signaling. We first compared the subcellular localization of TRPV1 in resting and activated CD4$^+$ T cells by confocal microscopy. We found that under resting conditions, TRPV1 localized together with components of the TCR complex, such as the coreceptor CD4 (**Fig. 1d**,**e**) and the Src-family tyrosine kinase Lck (**Fig. 4a**). In addition, Lck and TRPV1 were rapidly recruited to TCR clusters after ligation of the TCR (**Fig. 4a**). Since formation of the cap structure is known to be dependent on tyrosine phosphorylation[18,19], we investigated whether TRPV1 clustering was dependent on a similar mechanism. Indeed, we found that PP2, an inhibitor of the Src family of tyrosine kinases[20], inhibited capping of Lck and TRPV1 (**Fig. 4a**).

Because the phosphorylation of TRP channels regulates their channel activity[21–23], we investigated whether engagement of the TCR induced tyrosine phosphorylation of TRPV1^{CD4}. To address the possible role of Lck in this system, we examined the tyrosine-phosphorylation status of endogenous TRPV1 immunoprecipitated from wild-type Jurkat T cells (clone E6.1) and a derivative mutant of Jurkat T cells that lack Lck expression (J.CaM1.6)[24]. Stimulation of the TCR induced tyrosine-phosphorylation of TRPV1 in the parental wild-type E6.1 cell line but not in the mutant, Lck-deficient J.CaM1.6 cells (**Fig. 4b**). In accordance with published studies that have demonstrated an essential role for tyrosine kinases of the Src family in the activation of TRPV1 channels[21–23], we found that TRPV1^{CD4}-mediated Ca^{2+} influx was almost completely abolished in the absence of Lck (**Fig. 4c**). Collectively, these results suggested that TRPV1 is part of the proximal TCR signaling cascade and that tyrosine phosphorylation by Lck is a possible gating mechanism for TRPV1^{CD4} after stimulation of the TCR.

We next evaluated the effect of TRPV1 deficiency on TCR signaling. We found no difference in phosphorylation of the TCR-proximal signaling components Zap70, Lat (**Fig. 4d**) and PLC-γ1 (**Fig. 4e**), a slight difference in phosphorylation of the kinases Erk1/2 and p38, and less activation of the kinase Jnk (**Fig. 4f**) in *Trpv1*$^{-/-}$ CD4$^+$ T cells relative to that in wild-type CD4$^+$ T cells. Consistent with their decreased TCR-induced Ca^{2+} influx, *Trpv1*$^{-/-}$ CD4$^+$ T cells failed to sustain localization of NFAT-1 to the nucleus (**Fig. 4g**) and displayed reduced activation of NF-κB (**Fig. 4h**) upon stimulation of the TCR.

© 2014 Nature America, Inc. All rights reserved.

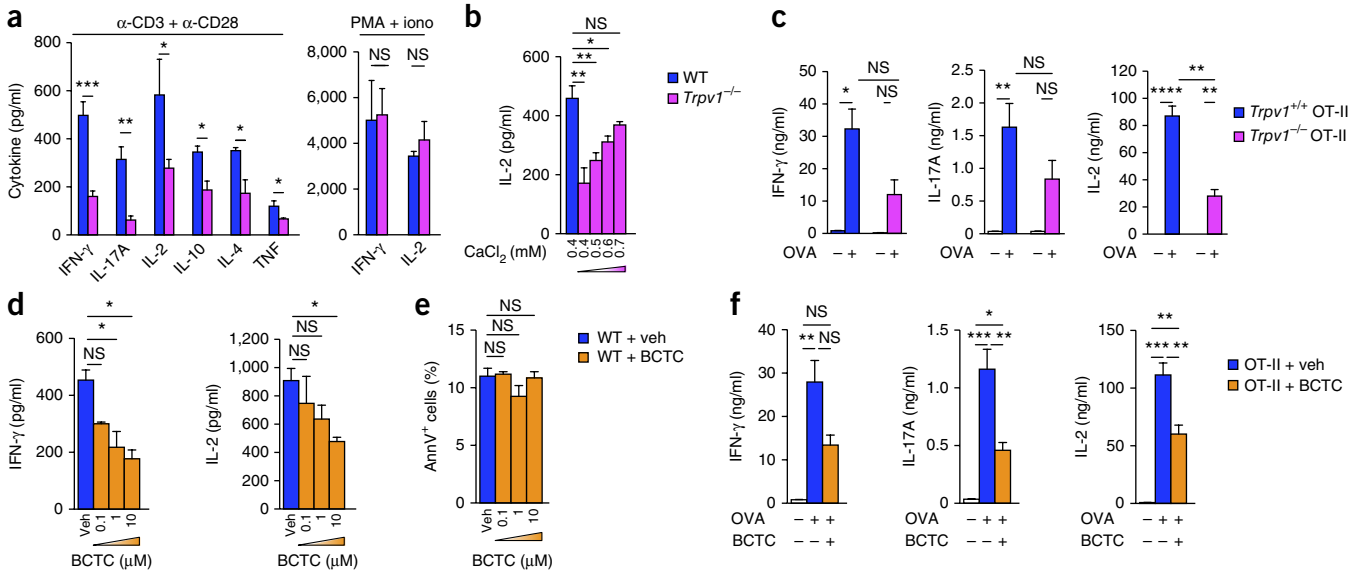

Figure 5 Genetic deletion or pharmacological inhibition of TRPV1^{CD4} decreases TCR-induced production of cytokines. (**a**) Enzyme-linked immunosorbent assay (ELISA) of cytokines (horizontal axes) in wild-type and *Trpv1*$^{-/-}$ splenic CD4$^+$ T cells stimulated for 24 h (IFN-γ, IL-17A, IL-2 and TNF) or 48 h (IL-10 and IL-4) with plate-bound anti-CD3 (10 μg/ml) and soluble anti-CD28 (1 μg/ml) (left; $n = 3$–6 mice per group) or with PMA (25 ng/ml) and ionomycin (500 nM) (right; $n = 3$ mice per group). (**b**) IL-2 in supernatants of wild-type and *Trpv1*$^{-/-}$ CD4$^+$ T cells ($n = 3$ mice per group) stimulated for 24 h with anti-CD3 plus anti-CD28 in RPMI medium supplemented with various concentrations (horizontal axis) of $CaCl_2$. (**c**) IFN-γ, IL-17A and IL-2 in supernatants of CD4$^+$ T cells recovered from cocultures of wild-type splenic CD11c$^+$ DCs loaded with OVA (OVA +) or not (OVA –) and incubated for 5 d with OVA-specific *Trpv1*$^{+/+}$ or *Trpv1*$^{-/-}$ OT-II splenic CD4$^+$ T cells ($n = 4$ mice per group); equal numbers of the CD4$^+$ T cells recovered were restimulated for 24 h with anti-CD3 plus anti-CD28 before analysis. (**d**) ELISA of IFN-γ and IL-2 in supernatants of wild-type splenic CD4$^+$ T cells ($n = 3$ mice per group) preincubated for 30 min with various concentrations of BCTC (TRPV1 inhibitor) or vehicle (Veh; 0.1% DMSO) and stimulated for 24 h with anti-CD3 plus anti-CD28. (**e**) Apoptosis of CD4$^+$ T cells among cells recovered in **d**, stained for CD4, annexin V (AnnV) and the DNA-intercalating dye 7-AAD, analyzed by flow cytometry. (**f**) Cytokine production by splenic OT-II CD4$^+$ T cells ($n = 4$ mice per group) pretreated for 30 min with 1 μM BCTC (+) or vehicle (0.1% DMSO) (–), then washed and cultured for 5 d together with wild-type splenic DCs loaded with OVA or not, followed by processing of CD4$^+$ T cells as in **c**. $^*P < 0.05$, $^{**}P < 0.01$, $^{***}P < 0.001$ and $^{****}P < 0.0001$ (two-tailed Student *t*-test (**a**) or one-way ANOVA with the *post-hoc* Bonferroni (**c**,**f**) or Dunnett's (**b**,**d**,**e**) test). Data are representative of five (**a**, left), three (**b**–**d**,**f**) or two (**a**, right, **e**) independent experiments (error bars, s.e.m.).

© 2014 Nature America, Inc. All rights reserved.

Thus, TRPV1^{CD4} seemed to be dispensable for proximal TCR signaling but was required for the proper transduction of distal TCR signaling events.

TRPV1^{CD4} contributes to TCR-induced cytokine production

We reasoned that the altered TCR signaling in *Trpv1*$^{-/-}$ CD4$^+$ T cells would affect their subsequent cytokine production. We observed that *Trpv1*$^{-/-}$ CD4$^+$ T cells produced lower concentrations of various cytokines (interferon-γ (IFN-γ), interleukin 17A (IL-17A), IL-2, IL-10, IL-4 and tumor-necrosis factor (TNF)) after stimulation with anti-CD3 and antibody to the coreceptor CD28 (anti-CD28) than did wild-type cells (**Fig. 5a**). We observed the opposite phenotype for *Trpv1*-TG CD4$^+$ T cells (**Supplementary Fig. 3a**). The diminished cytokine production by *Trpv1*$^{-/-}$ CD4$^+$ T cells was not explained by increased apoptosis or a lower proliferative response of these cells (**Supplementary Fig. 4**). Moreover, TCR-independent activation of *Trpv1*$^{-/-}$ and wild-type CD4$^+$ T cells with the phorbol ester PMA and ionomycin resulted in similar secretion of IFN-γ and IL-2 (**Fig. 5a**). Using IL-2 as a 'readout', we found that its diminished production by *Trpv1*$^{-/-}$ CD4$^+$ T cells was 'rescued' by an increase in the extracellular calcium concentration in the culture medium (**Fig. 5b**). These data suggested that the diminished cytokine production in *Trpv1*$^{-/-}$ CD4$^+$ T cells was probably due to the decreased TCR-induced Ca^{2+} influx observed in these cells (**Fig. 3** and **Supplementary Fig. 2**). In addition, in an antigen-specific model (OT-II cells, which have transgenic expression of an ovalbumin (OVA)-specific TCR), we found that *Trpv1*$^{-/-}$ OT-II CD4$^+$ T cells stimulated with OVA-loaded wild-type dendritic cells (DCs) had lower production of IFN-γ, IL-17A and IL-2 than did control (*Trpv1*$^{+/+}$) OT-II cells under the same stimulatory conditions (**Fig. 5c** and **Supplementary Fig. 3b**).

To further confirm the contribution of TRPV1^{CD4}-induced signaling to cytokine production, we treated wild-type CD4$^+$ T cells with the TRPV1 antagonist BCTC. BCTC decreased the release of cytokines from CD4$^+$ T cells in a concentration-dependent way upon stimulation with anti-CD3 plus anti-CD28 (**Fig. 5d**). The observed decrease in cytokine production was not due to an increase in the apoptosis of CD4$^+$ T cells (**Fig. 5e**). BCTC also significantly diminished cytokine production by OT-II CD4$^+$ T cells upon stimulation with OVA-loaded DCs (**Fig. 5f**). Together these results suggested a cell-intrinsic role for TRPV1^{CD4} in promoting TCR-induced cytokine production.

TRPV1 inhibition decreases human CD4$^+$ T cell activation

To explore the relevance of the data generated in the mouse to the human system, we determined the effect of pharmacological inhibition of TRPV1 on the activation profile of primary CD4$^+$ T cells enriched from the peripheral blood of healthy donors. We stimulated the cells with anti-CD3 plus anti-CD28 in the presence or absence of the TRPV1 antagonist SB366791. We analyzed upregulation of the surface expression of activation markers (i.e., CD25 and HLA-DR) 48 h later and found that SB366791 decreased their expression in a concentration-dependent way (**Fig. 6a**,**b**). Consistent with results obtained with the mouse

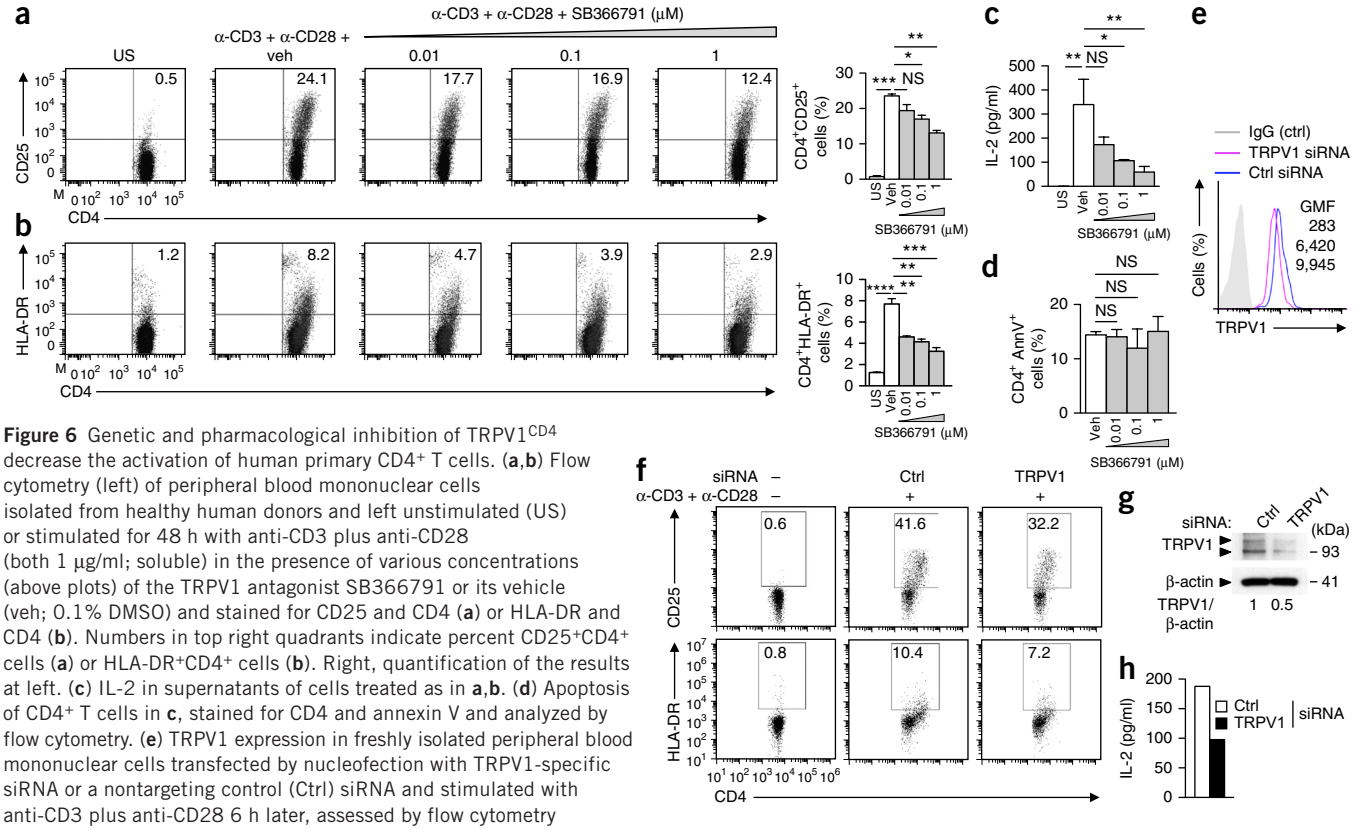

Figure 6 Genetic and pharmacological inhibition of TRPV1^{CD4} decrease the activation of human primary CD4$^+$ T cells. (**a**,**b**) Flow cytometry (left) of peripheral blood mononuclear cells isolated from healthy human donors and left unstimulated (US) or stimulated for 48 h with anti-CD3 plus anti-CD28 (both 1 μg/ml; soluble) in the presence of various concentrations (above plots) of the TRPV1 antagonist SB366791 or its vehicle (veh; 0.1% DMSO) and stained for CD25 and CD4 (**a**) or HLA-DR and CD4 (**b**). Numbers in top right quadrants indicate percent CD25$^+$CD4$^+$ cells (**a**) or HLA-DR$^+$CD4$^+$ cells (**b**). Right, quantification of the results at left. (**c**) IL-2 in supernatants of cells treated as in **a**,**b**. (**d**) Apoptosis of CD4$^+$ T cells in **c**, stained for CD4 and annexin V and analyzed by flow cytometry. (**e**) TRPV1 expression in freshly isolated peripheral blood mononuclear cells transfected by nucleofection with TRPV1-specific siRNA or a nontargeting control (Ctrl) siRNA and stimulated with anti-CD3 plus anti-CD28 6 h later, assessed by flow cytometry (numbers in plot as in **Fig. 1c**). (**f**) Expression of the surface activation markers CD25 and HLA-DR on gated CD4$^+$ T cells sorted from cells as in **e** at 48 h after transfection (42 h after stimulation), and in untransfected untreated cells (left). Numbers in outlined areas indicate percent CD25$^+$CD4$^+$ cells (top row) or HLA-DR$^+$CD4$^+$ cells (bottom row). (**g**,**h**) Immunoblot analysis of TRPV1 (**g**) and ELISA of IL-2 (**h**) in a human CD4$^+$ T cell clone 48 h after transfection and 42 h after stimulation as in **e**. $^*P < 0.05$, $^{**}P < 0.01$, $^{***}P < 0.001$ and $^{****}P < 0.0001$ (one-way ANOVA with *post-hoc* Dunnett's test). Data are representative of four independent experiments (**a**–**d**; mean and s.e.m. of two or three donors) or three independent experiments (with one donor (**e**–**h**)).

system, inhibition of TRPV1 also decreased IL-2 production (**Fig. 6c**). Notably, we observed this effect even at very low concentrations of the antagonist SB366791 (≥0.01 μM), and it was not associated with increased apoptosis of CD4$^+$ T cells (**Fig. 6d**). To confirm those findings, we knocked down TRPV1 in primary human CD4$^+$ T cells through the use of small interfering RNA (siRNA). Similar to pharmacological inhibition of TRPV1, knockdown of TRPV1 decreased the expression of CD25 and HLA-DR (**Fig. 6e**,**f**) and the production of IL-2 (**Fig. 6g**,**h**) upon stimulation with anti-CD3 plus anti-CD28. Collectively, these data indicated the TRPV1 channel contributed to the activation of human CD4$^+$ T cells.

TRPV1^{CD4} regulates proinflammatory CD4$^+$ T cell responses

To analyze the contribution of TRPV1-induced signaling to CD4$^+$ T cell responses *in vivo*, we applied two different models of CD4$^+$ T cell–mediated colitis. We first used the *Il10*$^{-/-}$ model[25] and compared the severity of colitis in *Il10*$^{-/-}$ mice and *Il10*$^{-/-}$*Trpv1*$^{-/-}$ mice. *Il10*$^{-/-}$ mice lost more weight than *Il10*$^{-/-}$*Trpv1*$^{-/-}$ mice did after the induction and synchronization of colitis by oral treatment with the nonselective cyclooxygenase inhibitor piroxicam[26] (**Fig. 7a**). Histological analysis of the colon confirmed that *Il10*$^{-/-}$ mice developed severe inflammation with epithelial hyperproliferation, crypt loss and cellular infiltration in the mucosa and submucosa, whereas we observed significantly lower inflammatory response in *Il10*$^{-/-}$*Trpv1*$^{-/-}$ mice (**Fig. 7b,c**). In addition, *Il10*$^{-/-}$ mice treated with the TRPV1 antagonist SB366791 showed attenuated colonic inflammation and T cell–derived production of inflammatory cytokines compared with that of *Il10*$^{-/-}$ mice treated with vehicle (**Supplementary Fig. 5**).

To confirm the cell-intrinsic role of TRPV1^{CD4} in intestinal inflammation, we transferred wild-type or *Trpv1*$^{-/-}$ naive (CD4$^+$CD45RB^{hi}CD25$^-$) T cells into recipient mice deficient in recombination-activating gene 1 (*Rag1*$^{-/-}$ mice) and assessed their ability to elicit colitis[25]. We used *Rag1*$^{-/-}$ recipients of wild-type naive CD4$^+$ T cells transferred together with regulatory T cells (T_{reg} cells) (CD4$^+$CD45RB^{lo}CD25$^+$) as a control. The adoptive transfer of wild-type naive CD4$^+$ T cells alone induced severe colitis in the recipients, as reflected by significant body weight loss, high disease activity index and histological signs of severe colitis (**Fig. 7d–g** and **Supplementary Fig. 6a**,**b**). We did not observe this after the transfer of *Trpv1*$^{-/-}$ naive CD4$^+$ T cells (**Fig. 7d–g** and **Supplementary Fig. 6a**,**b**). Massive cellular infiltration coincident with severe crypt loss was evident in the colons of *Rag1*$^{-/-}$ mice given transfer of wild-type naive CD4$^+$ T cells, but not in the colons of those given transfer of *Trpv1*$^{-/-}$ naive CD4$^+$ T cells (**Supplementary Fig. 6c**). To quantify the inflammatory cytokines produced in the colonic mucosa of these mice, we cultured colonic explants *ex vivo*. The colonic explants of *Rag1*$^{-/-}$ mice given transfer of wild-type naive CD4$^+$ T cells released more IFN-γ, IL-17A and TNF than did those from recipients of *Trpv1*$^{-/-}$ naive CD4$^+$ T cells (**Fig. 7h**). The abundance of mRNA encoding several proinflammatory cytokines (*Ifng, Il17a, Il22, Tnf* and *Il1b*) and chemokines (*Cxcl1, Cxcl9, Cxcl10, Ccl2* and *Ccl13*) was also lower in colon

© 2014 Nature America, Inc. All rights reserved.

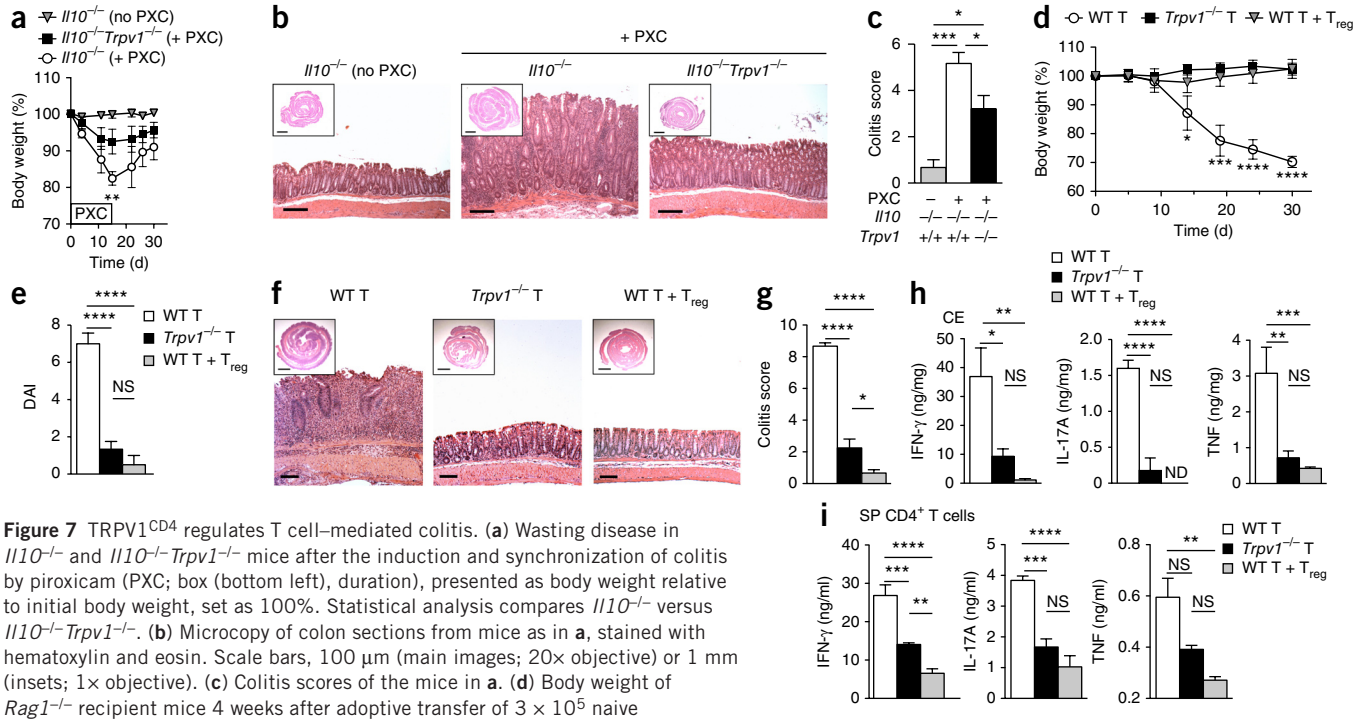

Figure 7 TRPV1^{CD4} regulates T cell–mediated colitis. (**a**) Wasting disease in *Il10*$^{-/-}$ and *Il10*$^{-/-}$*Trpv1*$^{-/-}$ mice after the induction and synchronization of colitis by piroxicam (PXC; box (bottom left), duration), presented as body weight relative to initial body weight, set as 100%. Statistical analysis compares *Il10*$^{-/-}$ versus *Il10*$^{-/-}$*Trpv1*$^{-/-}$. (**b**) Microcopy of colon sections from mice as in **a**, stained with hematoxylin and eosin. Scale bars, 100 μm (main images; 20× objective) or 1 mm (insets; 1× objective). (**c**) Colitis scores of the mice in **a**. (**d**) Body weight of *Rag1*$^{-/-}$ recipient mice 4 weeks after adoptive transfer of 3 × 10^5 naive (CD4$^+$CD45RB^{hi}CD25$^-$) T cells (sorted by flow cytometry) from wild-type mice (WT T) or *Trpv1*$^{-/-}$ mice (*Trpv1*$^{-/-}$ T) or a mixture of 3 × 10^5 wild-type naive CD4$^+$ T cells plus 1.5 × 10^5 wild-type (CD4$^+$CD45RB^{lo}CD25$^+$) T$_{reg}$ cells (WT T + T$_{reg}$), presented as in **a**; statistical analyses compare WT T versus *Trpv1*$^{-/-}$ T. (**e**) Disease activity index (DAI) of the mice in **d**. (**f**) Microcopy of colon sections from the mice in **d**, stained with hematoxylin and eosin. Scale bars, 100 μm (main images; 20× objective) or 1 mm (insets; 1× objective). (**g**) Colitis scores of the mice in **d**. (**h**) Cytokine concentrations in colonic explants (CE) from the mice in **d** after 24 h of culture. (**i**) Cytokine production by splenic CD4$^+$ T cells isolated from the mice in **d** and restimulated for 24 h with anti-CD3 (10 μg/ml, plate-bound) and anti-CD28 (1 μg/ml, soluble). $^*P < 0.05$, $^{**}P < 0.01$, $^{***}P < 0.001$ and $^{****}P < 0.0001$ (one-way (**c**,**e**,**g**–**i**) or two-way (**a**,**d**) ANOVA with the *post-hoc* Bonferroni test). Data are from one experiment representative of two experiments (mean and s.e.m. of $n = 6$–7 (**a**–**c**), 6–8 (**d**–**g**) or 4 (**h**,**i**) mice per group).

homogenates from recipients of *Trpv1*$^{-/-}$ CD4$^+$ T cells than in those of recipients of wild-type CD4$^+$ T cells (**Supplementary Fig. 6d**). The transferred *Trpv1*$^{-/-}$ CD4$^+$ T cells secreted significantly lower amounts of proinflammatory cytokines (IFN-γ, IL-17A and TNF) than did the transferred wild-type CD4$^+$ T cells (**Fig. 7i**). Moreover, the number of CD4$^+$ T cells producing IFN-γ, IL-17A or IL-10 was also much lower in the spleen, mesenteric lymph nodes and lamina propria of the recipients of *Trpv1*$^{-/-}$ naive CD4$^+$ T cells than in those of the recipients of wild-type naive CD4$^+$ T cells (**Supplementary Fig. 7**). This suggested that the decreased colitogenicity of *Trpv1*$^{-/-}$ naive CD4$^+$ T cells was possibly due to defective activation and differentiation *in situ*. In line with this hypothesis, we found that *Trpv1*$^{-/-}$ OT-II naive CD4$^+$ T cells were less able to differentiate into effector cells of the T$_H$1, T$_H$2 and T$_H$17 subsets of helper T cells *in vitro* than were control (*Trpv1*$^{+/+}$) OT-II naive cells (**Supplementary Fig. 8**).

To analyze the potential contribution of TRPV1 to other cell types in the recipients, we compared the colitis induced by the transfer of wild-type naive CD4$^+$ T cells into *Rag1*$^{-/-}$ mice with that induced in *Rag1*$^{-/-}$ *Trpv1*$^{-/-}$ recipients. We found that *Rag1*$^{-/-}$ and *Rag1*$^{-/-}$*Trpv1*$^{-/-}$ recipients developed similar body weight loss and colonic inflammation and displayed similar proinflammatory CD4$^+$ T cell responses (**Fig. 8**). Finally, in line with their enhanced activation profile *in vitro* (**Supplementary Fig. 3a**), *Trpv1*-TG naive CD4$^+$ T cells induced exacerbated colitis after transfer into *Rag1*$^{-/-}$ recipients (**Supplementary Fig. 9**). Together these results demonstrated a cell-intrinsic role of TRPV1^{CD4} in promoting the activation and inflammatory responses of T cells (proposed model for the regulation of T cell activation by TRPV1, **Supplementary Fig. 10**).

DISCUSSION

While Ca^{2+} release–activated Ca^{2+} channels have been described as the major source for the entry of Ca^{2+} into T cells[1,3], several additional families of channels expressed on the plasma membrane of T cells may have important roles in this process, including voltage-gated Ca^{2+} channels and TRP channels[2,5,6]. In particular, the contribution of TRP channels to this process is not well defined. TRP channels may decrease Ca^{2+} influx in T cells (for example, TRPM4)[27] or increase such influx (for example, TRPC3)[7,28], and it is as yet unclear whether they directly affect TCR signaling and T cell activation.

In the present study, we found that the TRPV1 channel was functionally expressed in CD4$^+$ T cells (TRPV1^{CD4}) and reported a previously unknown function for TRPV1 beyond its well-recognized role as a pain receptor[10,29]. Our results indicated an essential role for TRPV1^{CD4} in the activation and the acquisition of inflammatory properties by CD4$^+$ T cells. TRPV1 expression has been reported in peripheral blood lymphocytes in rats[30] and in humans[7,31–34], but the functionality of the TRPV1 channel was not assessed and it remained unknown whether TRPV1 has a role in the activation and function of T cells. In this study, we demonstrated that TRPV1 was constitutively expressed in mouse and human CD4$^+$ T cells as well as in the Jurkat human leukemic T cell line. By whole-cell patch clamp, we demonstrated the functionality of the TRPV1 channel at the plasma membrane and recorded capsaicin-induced currents in wild-type CD4$^+$ T cells but not in *Trpv1*$^{-/-}$ CD4$^+$ T cells. The smaller TRPV1 current observed in CD4$^+$ T cells than that reported before in sensory neurons or in cells with heterologous overexpression of TRPV1 might account for the following cell-intrinsic factors: lower

© 2014 Nature America, Inc. All rights reserved.

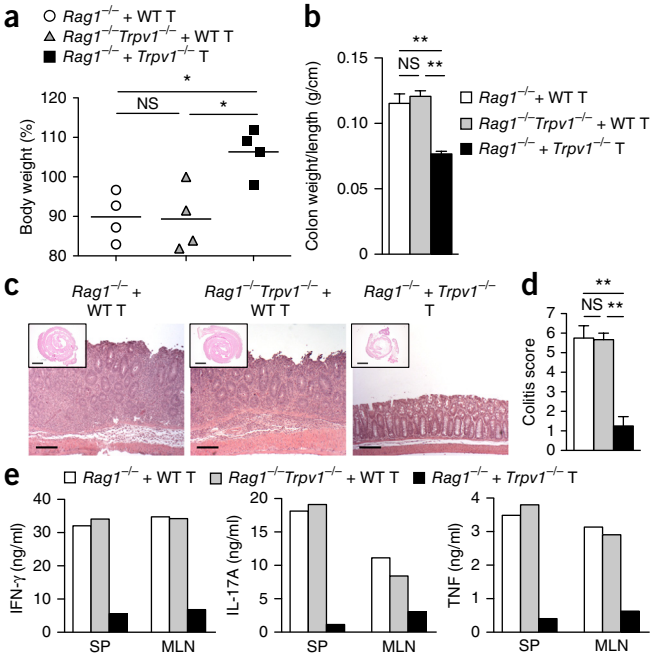

Figure 8 TRPV1 expression in non-CD4$^+$ T cells does not affect colitis severity in an adoptive-transfer model. (**a**) Body weight of *Rag1*$^{-/-}$ or *Rag1*$^{-/-}$*Trpv1*$^{-/-}$ recipient mice 4 weeks after transfer of 3 × 10^5 wild-type or *Trpv1*$^{-/-}$ naive (CD4$^+$CD45RB^{hi}CD25$^-$) T cells (sorted by flow cytometry), presented relative to initial body weight, set as 100%. (**b**) Colon weight of the mice in **a**, presented as a ratio to colon length. (**c**) Microcopy of colon sections from mice as in **a**, stained with hematoxylin and eosin. Scale bars, 100 μm (main images; 20× objective) or 1 mm (insets; 1× objective). (**d**) Colitis scores of the mice in **a**. (**e**) ELISA of cytokines in pooled splenic (SP) and mesenteric lymph node (MLN) CD4$^+$ T cells at 24 h after restimulation with anti-CD3 (10 μg/ml plate-bound) and anti-CD28 (1 μg/ml soluble). $^*P < 0.05$ and $^{**}P < 0.001$ (one-way ANOVA with the *post-hoc* Bonferroni test). Data are representative of two independent experiments (mean and s.e.m. of four mice per group).

TRPV1 expression in CD4$^+$ T cells than in cells with heterologous overexpression of TRPV1; different post-translational modifications (for example, phosphorylation and glycosylation) that could increase the TRPV1-activation threshold and result in a lower sensitivity to capsaicin; and/or the presence of different regulatory proteins associated with TRPV1^{CD4} (refs. 22,35,36). Nonetheless, it is well known that even small currents can produce physiologically important increases in $[Ca^{2+}]_i$ and have profound consequences on cell physiology[37]. Accordingly, by Ca^{2+} imaging and flow cytometry–based Ca^{2+}-monitoring techniques, we identified TRPV1^{CD4} as a functional Ca^{2+} channel and showed that it contributed to TCR-induced Ca^{2+} influx in a manner independent of store-operated Ca^{2+} entry. We also confirmed the contribution of TRPV1 to TCR-induced Ca^{2+} currents by whole-cell patch clamp and found that crosslinking of TCRs produced significantly smaller inward currents in *Trpv1*$^{-/-}$ CD4$^+$ T cells than in wild-type cells.

Our results suggest that TRPV1 is a component of the TCR signaling complex, since it is rapidly recruited to TCR clusters upon TCR stimulation in a Src-dependent manner. Through the use of a Jurkat cell clone that lacks expression of the Src-family kinase Lck[24], we showed that Lck rapidly tyrosine-phosphorylated TRPV1 after stimulation via the TCR and regulated TRPV1^{CD4} channel activity. Tyrosine phosphorylation by Src kinase has been shown to be essential for the activation of TRPV1 channels in other cell types. Indeed, capsaicin-induced currents in dorsal root ganglion neurons are blocked by the Src-family kinase inhibitor PP2 and are enhanced by the tyrosine phosphatase inhibitor sodium orthovanadate. PP2 also abolishes currents in HEK293 cells transfected to express rat TRPV1, whereas cotransfection of cells to express TRPV1 with an activated Src kinase (v-Src) results in fivefold increase in capsaicin-induced currents[21]. Finally, in cells transfected to express a dominant-negative non-receptor (c-Src) tyrosine kinase, capsaicin-induced currents are considerably diminished[21,23]. This mode of activation by Src-family kinases is not restricted to TRPV1 and has also been shown for other members of the TRP family[22]. Our findings are therefore consistent with the reported protein-protein interaction of TRPV1 and Src and emphasize the role of Src-family kinases in regulating the activity of TRPV1 channels[21–23]. Tyrosine-phosphorylation by Lck is therefore a possible gating mechanism for TRPV1^{CD4} after stimulation of the TCR.

Analysis of TCR signaling in wild-type and *Trpv1*$^{-/-}$ CD4$^+$ T cells revealed diminished activation of the p38 and Jnk pathways and less translocation of NF-κB to the nucleus in *Trpv1*$^{-/-}$ CD4$^+$ T cells. In line with their decreased TCR-induced Ca^{2+} influx, *Trpv1*$^{-/-}$ CD4$^+$ T cells also failed to maintain localization of NFAT-1 to the nucleus after stimulation via the TCR. Consequently, *Trpv1*$^{-/-}$ CD4$^+$ T cells displayed a significantly diminished cytokine-production profile after either antigen-specific stimulation (OVA-loaded DCs) or nonspecific stimulation (with anti-CD3 plus anti-CD28). Collectively, these data indicated that TRPV1 was necessary for proper TCR-induced signaling and cytokine production but was dispensable for CD4$^+$ T cell proliferation under our experimental conditions.

Consistent with our *in vitro* data, we found a role for TRPV1^{CD4} in T cell inflammatory responses *in vivo* in two different models of inflammatory bowel disease. *Il10*$^{-/-}$*Trpv1*$^{-/-}$ mice and *Il10*$^{-/-}$ mice treated with a TRPV1 antagonist had less colonic inflammation than did untreated *Il10*$^{-/-}$ control mice. In addition, *Trpv1*$^{-/-}$ naive CD4$^+$ T cells had an impaired ability to elicit colitis when transferred into *Rag1*$^{-/-}$ recipients. As the activation of TRPV1 in sensory afferents contributes to neurogenic inflammation, which might affect the severity of colitis[38], we compared the colitis induced by the transfer of wild-type naive CD4$^+$ T cells into *Rag1*$^{-/-}$ mice with that induced in *Rag1*$^{-/-}$*Trpv1*$^{-/-}$ recipient mice. Genetic deletion of TRPV1 in donor CD4$^+$ T cells determined the severity of colonic inflammation in this model, but genetic deletion of TRPV1 in other cells of the recipients did not. The T cell–intrinsic role of TRPV1 was further demonstrated by the enhanced activation profile and proinflammatory properties of *Trpv1*-TG CD4$^+$ T cells.

Finally, our results indicated that inhibition of TRPV1^{CD4} in mouse and human CD4$^+$ T cells with TRPV1 antagonists or with TRPV1-specific siRNA recapitulated the phenotype of *Trpv1*$^{-/-}$ CD4$^+$ T cells. As TRPV1 functions as a nociceptor (i.e., pain receptor) in sensory neurons[29], TRPV1 antagonists were developed as analgesic agents[39]. The immunomodulatory properties of TRPV1 antagonists identified in our study suggest that their application might be beneficial in patients with CD4$^+$ T cell–mediated immunopathologies such as inflammatory bowel disease.

METHODS

Methods and any associated references are available in the online version of the paper.

© 2014 Nature America, Inc. All rights reserved.

Note: Any Supplementary Information and Source Data files are available in the online version of the paper.

ACKNOWLEDGMENTS

We thank C. Conche and K. Sauer for help with measurements of Ca^{2+}; A. Patapoutian (The Scripps Research Institute) for Chinese hamster ovary cells transfected to express TRPV1; E. Garcia and T. Snutch for access to electrophysiological equipment; J. Lee and C. Quinley for discussions; M. Scholl for animal breeding; T. Rambaldo for cell sorting; S. Shenouda for tissue processing; N. Varki and L. Eckmann for help with histological evaluations; and J. Santini for technical assistance with confocal imaging at the Neuroscience microscopy shared facility of the University of California San Diego (supported by the National Institute of Neurological Disorders and Stroke of the US National Institutes of Health (P30 NS047101)). Supported by the US National Institutes of Health (U01 AI095623 and P01 DK35108 to E.R., and AI083432 to Y.G.), the Canadian Institutes of Health Research (MOP-102698 to W.A.J.), the Broad Foundation (IBD-0342R to E.R.), the Crohn's & Colitis Foundation of America (SRA 3038 to E.R., RFA 3574 to S.B., and RFA 2927 to P.R.d.J.), the European Molecular Biology Organization (ALTF 288-2009 to S.B.), the Fulbright Association (S.B.), the Philippe Foundation (S.B.) and the Japan Society for the Promotion of Science (Y.A.-N.).

AUTHOR CONTRIBUTIONS

S.B., P.R.d.J., A.F. and E.R. designed the study; S.B., Y.A.-N., P.R.d.J., K.T., L.A., T.Y., T.H., X.L. and J.M.G.-N. performed most of the *in vitro* and *in vivo* experiments; S.B. measured the Ca^{2+} flux by flow cytometry, with the technical assistance of X.L. and G.F.; S.S. and Y.G. performed single-cell Ca^{2+} imaging in mouse $CD4^+$ T cells; S.B. and J.L., with the help of H.D., performed single-cell Ca^{2+} imaging in Jurkat cells; L.L.N., H.X., S.R.S. and W.A.J. planned and designed the electrophysiological assays, L.L.N., H.X. and S.R.S. performed these assays, and L.L.N., H.X., S.R.S. and W.A.J. wrote the corresponding sections of the manuscript; R.T. and A.F. performed the human T cell experiments with TRPV1 antagonists; S.H. and M.C. took care of the mouse colony and genotyped the mice; L.L.N., H.X., S.R.S., W.A.J., S.B., Y.A.-N., P.R.d.J., T.Y., K.T., L.A., A.F. and E.R. analyzed and interpreted the data; S.B., E.R. and W.A.J. revised the manuscript for publication; and S.B. and E.R. wrote the manuscript.

COMPETING FINANCIAL INTERESTS

The authors declare competing financial interests: details are available in the online version of the paper.

Reprints and permissions information is available online at http://www.nature.com/reprints/index.html.

1. Oh-hora, M. & Rao, A. Calcium signaling in lymphocytes. *Curr. Opin. Immunol.* **20**, 250–258 (2008).
2. Gallo, E.M., Cante-Barrett, K. & Crabtree, G.R. Lymphocyte calcium signaling from membrane to nucleus. *Nat. Immunol.* **7**, 25–32 (2006).
3. Hogan, P.G., Lewis, R.S. & Rao, A. Molecular basis of calcium signaling in lymphocytes: STIM and ORAI. *Annu. Rev. Immunol.* **28**, 491–533 (2010).
4. Omilusik, K. *et al.* The Ca(v)1.4 calcium channel is a critical regulator of T cell receptor signaling and naive T cell homeostasis. *Immunity* **35**, 349–360 (2011).
5. Omilusik, K.D., Nohara, L.L., Stanwood, S. & Jefferies, W.A. Weft, warp, and weave: the intricate tapestry of calcium channels regulating T lymphocyte function. *Front. Immunol.* **4**, 164 (2013).
6. Schwarz, E.C. *et al.* TRP channels in lymphocytes. *Handb. Exp. Pharmacol.* **179**, 445–456 (2007).
7. Wenning, A.S. *et al.* TRP expression pattern and the functional importance of TRPC3 in primary human T-cells. *Biochim. Biophys. Acta* **1813**, 412–423 (2011).
8. Venkatachalam, K. & Montell, C. TRP channels. *Annu. Rev. Biochem.* **76**, 387–417 (2007).
9. Owsianik, G., Talavera, K., Voets, T. & Nilius, B. Permeation and selectivity of TRP channels. *Annu. Rev. Physiol.* **68**, 685–717 (2006).
10. Caterina, M.J. *et al.* The capsaicin receptor: a heat-activated ion channel in the pain pathway. *Nature* **389**, 816–824 (1997).
11. Touska, F., Marsakova, L., Teisinger, J. & Vlachova, V. A "cute" desensitization of TRPV1. *Curr. Pharm. Biotechnol.* **12**, 122–129 (2011).
12. Gunthorpe, M.J. *et al.* Identification and characterisation of SB-366791, a potent and selective vanilloid receptor (VR1/TRPV1) antagonist. *Neuropharmacology* **46**, 133–149 (2004).
13. Arenkiel, B.R., Klein, M.E., Davison, I.G., Katz, L.C. & Ehlers, M.D. Genetic control of neuronal activity in mice conditionally expressing TRPV1. *Nat. Methods* **5**, 299–302 (2008).
14. Parekh, A.B. & Penner, R. Store depletion and calcium influx. *Physiol. Rev.* **77**, 901–930 (1997).
15. Smith, G.D. *et al.* TRPV3 is a temperature-sensitive vanilloid receptor-like protein. *Nature* **418**, 186–190 (2002).
16. Valenzano, K.J. *et al.* N-(4-tertiarybutylphenyl)-4-(3-chloropyridin-2-yl)tetrahydropyrazine-1(2H)-carbox-amide (BCTC), a novel, orally effective vanilloid receptor 1 antagonist with analgesic properties: I. *in vitro* characterization and pharmacokinetic properties. *J. Pharmacol. Exp. Ther.* **306**, 377–386 (2003).
17. Wahl, P., Foged, C., Tullin, S. & Thomsen, C. Iodo-resiniferatoxin, a new potent vanilloid receptor antagonist. *Mol. Pharmacol.* **59**, 9–15 (2001).
18. Barr, V.A., Bernot, K.M., Shaffer, M.H., Burkhardt, J.K. & Samelson, L.E. Formation of STIM and Orai complexes: puncta and distal caps. *Immunol. Rev.* **231**, 148–159 (2009).
19. Oh-hora, M. Calcium signaling in the development and function of T-lineage cells. *Immunol. Rev.* **231**, 210–224 (2009).
20. Hanke, J.H. *et al.* Discovery of a novel, potent, and Src family-selective tyrosine kinase inhibitor. Study of Lck- and FynT-dependent T cell activation. *J. Biol. Chem.* **271**, 695–701 (1996).
21. Jin, X. *et al.* Modulation of TRPV1 by nonreceptor tyrosine kinase, c-Src kinase. *Am. J. Physiol. Cell Physiol.* **287**, C558–C563 (2004).
22. Yao, X., Kwan, H.Y. & Huang, Y. Regulation of TRP channels by phosphorylation. *Neurosignals* **14**, 273–280 (2005).
23. Zhang, X., Huang, J. & McNaughton, P.A. NGF rapidly increases membrane expression of TRPV1 heat-gated ion channels. *EMBO J.* **24**, 4211–4223 (2005).
24. Straus, D.B. & Weiss, A. Genetic evidence for the involvement of the lck tyrosine kinase in signal transduction through the T cell antigen receptor. *Cell* **70**, 585–593 (1992).
25. Wirtz, S. & Neurath, M.F. Mouse models of inflammatory bowel disease. *Adv. Drug Deliv. Rev.* **59**, 1073–1083 (2007).
26. Berg, D.J. *et al.* Rapid development of colitis in NSAID-treated IL-10-deficient mice. *Gastroenterology* **123**, 1527–1542 (2002).
27. Launay, P. *et al.* TRPM4 regulates calcium oscillations after T cell activation. *Science* **306**, 1374–1377 (2004).
28. Philipp, S. *et al.* TRPC3 mediates T-cell receptor-dependent calcium entry in human T-lymphocytes. *J. Biol. Chem.* **278**, 26629–26638 (2003).
29. Caterina, M.J. *et al.* Impaired nociception and pain sensation in mice lacking the capsaicin receptor. *Science* **288**, 306–313 (2000).
30. Schumacher, M.A., Moff, I., Sudanagunta, S.P. & Levine, J.D. Molecular cloning of an N-terminal splice variant of the capsaicin receptor. Loss of N-terminal domain suggests functional divergence among capsaicin receptor subtypes. *J. Biol. Chem.* **275**, 2756–2762 (2000).
31. Saunders, C.I., Kunde, D.A., Crawford, A. & Geraghty, D.P. Expression of transient receptor potential vanilloid 1 (TRPV1) and 2 (TRPV2) in human peripheral blood. *Mol. Immunol.* **44**, 1429–1435 (2007).
32. Engler, A. *et al.* Expression of transient receptor potential vanilloid 1 (TRPV1) in synovial fibroblasts from patients with osteoarthritis and rheumatoid arthritis. *Biochem. Biophys. Res. Commun.* **359**, 884–888 (2007).
33. Spinsanti, G. *et al.* Quantitative real-time PCR detection of TRPV1–4 gene expression in human leukocytes from healthy and hyposensitive subjects. *Mol. Pain* **4**, 51 (2008).
34. Bachiocco, V. *et al.* Lymphocyte TRPV 1–4 gene expression and MIF blood levels in a young girl clinically diagnosed with HSAN IV. *Clin. J. Pain* **27**, 631–634 (2011).
35. Shin, J.S. *et al.* Differences in sensitivity of vanilloid receptor 1 transfected to human embryonic kidney cells and capsaicin-activated channels in cultured rat dorsal root ganglion neurons to capsaicin receptor agonists. *Neurosci. Lett.* **299**, 135–139 (2001).
36. Voolstra, O. & Huber, A. Post-translational modifications of TRP channels. *Cells* **3**, 258–287 (2014).
37. Armstrong, D.L., Erxleben, C. & White, J.A. Patch clamp methods for studying calcium channels. *Methods Cell Biol.* **99**, 183–197 (2010).
38. Gad, M., Pedersen, A.E., Kristensen, N.N., Fernandez Cde, F. & Claesson, M.H. Blockage of the neurokinin 1 receptor and capsaicin-induced ablation of the enteric afferent nerves protect SCID mice against T-cell-induced chronic colitis. *Inflamm. Bowel Dis.* **15**, 1174–1182 (2009).
39. Moran, M.M., McAlexander, M.A., Biro, T. & Szallasi, A. Transient receptor potential channels as therapeutic targets. *Nat. Rev. Drug Discov.* **10**, 601–620 (2011).
40. Kedei, N. *et al.* Analysis of the native quaternary structure of vanilloid receptor 1. *J. Biol. Chem.* **276**, 28613–28619 (2001).

© 2014 Nature America, Inc. All rights reserved.

ONLINE METHODS

Reagents and antibodies. For immunoblot analysis, we used the following antibodies: antibody to phosphorylated Erk1/2 (D13.14.4E), antibody to phosphorylated p38 (D3F9), antibody to phosphorylated Jnk (81E11), anti-Erk1/2 (137F5), anti-p38 (9212), anti-Jnk (9252), antibody to Zap70 phosphorylated at Tyr319 (2701) and antibody to PLC-γ1 phosphorylated at Tyr783 (2821; all from Cell Signaling Technology); antibody to Lat phosphorylated at Tyr191 (07-278) and antibody to phosphorylated tyrosine (4G-10; both from Millipore); anti-CD3ε (M-20; sc-1127), anti-Lck (2102; sc-13) and anti-TRPV1 (P-19; sc-12498; all from Santa Cruz Biotechnology); anti-TRPV1 (ACC-030; Alomone); monoclonal anti-NFAT1 (ab2722; Abcam); and anti-β-actin (AC-74; Sigma). For immunofluorescence studies, we used anti-TRPV1 (sc-12498; Santa Cruz Biotechnology), anti-Lck (sc-13; Santa Cruz Biotechnology), anti-CD4 (GK1.5; eBioscience), anti-CD45 (30-F11; BD Biosciences) and anti-claudin-3 (RB-9251; Thermo Scientific). For T cell stimulation, we used monoclonal anti–mouse CD3ε (145-2c11) and anti–mouse CD28 (PV-1; both from BioXcell), and monoclonal anti–human CD3ε (UCHT1) and anti–human CD28 (CD28.2; both from eBioscience). Other reagents included the following: PMA (phorbol 12-myristate 13-acetate), ionomycin, thapsigargin and phytohemagglutinin (all from Sigma); PP2 (Cayman Chemical); BCTC (N-(4-tertiarybutylphenyl)-4-(3-chloropyridin-2-yl)tetrahydropyrazine-1(2H)-carbox-amide) and I-RTX (iodo-resiniferatoxin) (Tocris); SB366791 (Enzo Life Sciences); an annexin-V and 7-amino-actinomycin D (7-AAD) apoptosis-detection kit (BD Biosciences); and CFSE (carboxyfluorescein diacetate succinimidyl ester), Indo-1 AM, and Fura-2 AM (Invitrogen).

Isolation of mRNA and quantitative PCR. RNA was isolated with an RNeasy Mini Kit according to the manufacturer's protocol (Qiagen). 1 μg of RNA sample was used for reverse transcription and synthesis of cDNA with qScript cDNA superMix (Quanta Biosciences). Quantitative real-time PCR was performed on an AB7300 (Applied Bisosytems) with PerfeCTa SYBR Green FastMix (Quanta Biosciences). Primers for specific target genes were designed on the basis of their reported sequences and were synthesized by IDT Technologies (sequences, **Supplementary Tables 1** and **2**). The expression of genes encoding several TRP channels in mouse CD4$^+$ T cells was compared after verification that amplification efficiencies for the different target genes were similar. For analysis of TRPV1 expression, quantitative PCR products were separated by electrophoresis through a 2% agarose gel, followed by staining with SYBR Safe DNA (Invitrogen) for further confirmation of the specificity of the primers used.

Mice. Six- to ten-week-old mice were used for all experimental procedures. Specific pathogen–free C57BL/6 (B6) mice were from Harlan Sprague Dawley or were bred in the animal facility of the Stein Clinical Research building at the University of California, San Diego. *Trpv1*$^{-/-}$ mice[29], *Trpv3*$^{-/-}$ mice[41], mice expressing *Trpv1* from the *Rosa26* locus[13], mice expressing Cre from the *Cd4* promoter (*Cd4*-Cre), *Rag1*$^{-/-}$ mice and OT-II mice on the B6 background (all from the Jackson Laboratories) were bred in the animal facility of the Stein Clinical Research building. For the generation of *Trpv1*$^{-/-}$ OT-II mice, *Il10*$^{-/-}$*Trpv1*$^{-/-}$ mice or *Rag*$^{-/-}$*Trpv1*$^{-/-}$ mice, *Trpv1*$^{-/-}$ mice were intercrossed with OT-II mice, *Il10*$^{-/-}$ mice or *Rag1*$^{-/-}$ mice respectively. Mice with *Cd4*-Cre–driven expression of a transgene encoding TRPV1 (*Trpv1*-TG) were generated by crossing of mice with alleles for *ROSA*-stop^{flox}-*TRPV1*-IRES-ECFP (which express *Trpv1* from the *Rosa26* locus) and *Cd4*-Cre in the animal facility of the Stein Clinical Research building. Mice were bred for more than 6 months and were genotyped before they were used in any experiments. All experimental procedures were conducted in accordance with institutional guidelines for animal care and use of the University of California, San Diego.

Isolation and stimulation of CD4$^+$ T cells. Mouse CD4$^+$ T cells were isolated from the spleen or mesenteric lymph nodes with a CD4$^+$ T cell negative selection kit (19752; StemCell). Purity of the enriched populations was controlled by staining with anti-CD4 (GK1.5; eBioscience) and anti-TCRβ (H57-597; eBioscience) by flow cytometry and was typically >94% for CD4$^+$ T cells derived from the spleen and >97% for CD4$^+$ T cells derived from the mesenteric lymph nodes. For ELISA, CD4$^+$ T cells were stimulated with 10 μg/ml plate-bound anti-CD3 (145-2c11; BioXcell) and 1 μg/ml soluble anti-CD28 (PV-1; BioXcell) in RPMI-1640 medium supplemented with 10% heat-inactivated FCS, 2 mM l-glutamine, 100 U/ml penicillin and 100 μg/ml streptomycin. Culture supernatants were collected at 24 h and 48 h for analysis of cytokine production (ELISA kits; eBioscience). For signaling experiments, CD4$^+$ T cells were stimulated for various times (for example, 0, 15, 30 or 60 min) with 5 μg/ml anti-CD3 and 2 μg/ml anti-CD28 (both soluble; antibodies identified above). Splenic CD4$^+$ T cells from OT-II or *Trpv1*$^{-/-}$ OT-II mice were isolated as described above. Bone marrow–derived DCs were cultured and harvested as described[42]. CD11c$^+$ bone marrow–derived DCs or splenic DCs were isolated with a CD11c$^+$ positive selection kit (18758; StemCell) and then were loaded for 2 h with 10 μg/ml of I-A^d-restricted OVA peptide (amino acids 323-339 (ISQAVHAAHAEINEAGR); PeptidoGenic Research) before the addition of wild-type or *Trpv1*$^{-/-}$ OT-II CD4$^+$ T cells to the culture (DC/T cell ratio, 1:2). After 5 d of coculture, CD4$^+$ T cells were recovered and then were restimulated for 24 h with anti-CD3 plus anti-CD28 (identified above). Supernatants were then collected and cytokines were measured by ELISA. For experiments with primary human CD4$^+$ T cells, peripheral blood mononuclear cells (PBMCs) were isolated from the blood of healthy donors by a Ficoll density-gradient technique. For some experiments, CD4$^+$ T cells had been isolated from the PBMCs and their populations expanded with phytohemagglutinin and allogeneic irradiated feeder cells (1×10^5 cells per well) as described[43]. The CD4$^+$ T cell clones or the PBMCs were left untreated or were treated with the TRPV1 antagonist SB366791 and were stimulated for 48 h with antibody to human CD3 (UCHT1; eBioscience) and antibody to human CD28 (CD28.2; eBioscience) (both 1 μg/ml; soluble) in RPMI-1640 medium. For analysis of phosphorylation of TRPV1 by immunoblot, Jurkat T cells (clones E6.1 and J.Cam1.6; American Type Culture Collection) were grown in complete RPMI-1640 medium (supplemented with 5% heat-inactivated FCS, 2 mM L-glutamine, 100 U/ml penicillin, and 100 μg/ml streptomycin) and were stimulated for the appropriate time with soluble antibody to human CD3 (2.5 μg/ml; OKT3; BioLegend) and antibody to human CD28 (1 μg/ml; CD28.2; eBioscience).

***In vitro* T cell differentiation.** CD4$^+$CD25$^-$ (naive) T cells were isolated from the spleen of wild-type OT-II or *Trpv1*$^{-/-}$ OT-II mice, and bone marrow–derived DCs were loaded for 24 h at 37 °C with OVA peptide (10 μg/ml; amino acids 323–339) and were γ-irradiated (30 Gy from a ^{137}Cs source). Those cells were cultured together (at a density of 1×10^6 T cells per well and 5×10^5 DCs per well) in flat-bottomed 24-well plates in complete RPMI medium (unless indicated otherwise) in the presence of the following: for T_H1 differentiation, recombinant mouse IL-12 (10 ng/ml; eBioscience) and neutralizing anti-IL-4 (10 μg/ml; BVD6-24G2; BioXcell); for T_H2 differentiation, recombinant mouse IL-4 (10 ng/ml), neutralizing anti-IFN-γ (10 μg/ml; XMG1.2; BioXcell) and neutralizing anti-IL-12 (10 μg/ml; R1-5D9; BioXcell); for T_H17 differentiation, recombinant mouse IL-6 (20 ng/ml) and TGF-β (4 ng/ml; both from eBioscience), plus neutralizing anti-IFN-γ (10 μg/ml; XMG1.2; BioXcell) and anti-IL-4 (10 μg/ml; BVD6-24G2; BioXcell) in complete IMDM; and for T_{reg} cell differentiation, recombinant mouse TGF-β (10 ng/ml; eBioscience) and IL-2 (20 ng/ml; eBioscience). At day 2, recombinant mouse IL-2 (10 ng/ml) was added to the T_H1 and T_H2 cultures. After 4 d, CD4$^+$ T cells were recovered and then were restimulated for 5 h or not with 10 μg/ml plate-bound anti-CD3 and 1 μg/ml soluble anti-CD28 (antibodies identified above) in the presence of GolgiStop (BD Biosciences). Intracellular cytokines were measured with anti-IFN-γ (XMG1.2), anti-IL-4 (11B11), anti-IL-17A (eBio17B7) and anti-IL-10 (JES5-16E3) according to the manufacturer's instructions (eBioscience).

Knockdown of TRPV1. Primary human CD4$^+$ T cell clones or freshly isolated PBMCs were transfected with 400 nM TRPV1-specific siRNA (a pool of three different siRNA duplexes; sc-36826; Santa Cruz Biotechnology) or control siRNA (Non-Targeting siRNA #1; Dharmacon) at a density of 5×10^6 cells per 100 μl human T cell nucleofector solution (VPA-1002; Lonza) with the Amaxa Nucleofector II device (program U-014; Lonza). After nucleofection, cells were immediately transferred into prewarmed complete RPMI-1640 and were cultured in a 24-well plate at 37 °C in a 5% CO2 humidified incubator. Six hours after transfection, cells were stimulated for a further 42 h with antibody to human CD3 and antibody to human CD28 (identified above; both 1 μg/ml, soluble). TRPV1-knockdown efficiency in cells was then analyzed (by flow

© 2014 Nature America, Inc. All rights reserved.

doi:10.1038/ni.3009

cytometry and immunoblot analysis), as was upregulation of the expression of the surface activation markers CD25 and HLA-DR (by flow cytometry) and cytokine IL-2 production (by ELISA). For knockdown of TRPV1 in Jurkat T cells (clone E6.1), cells were stably transduced with lentiviral particles expressing TRPV1-specific short hairpin RNA (sc-36826-V) or with copGFP control lentiviral particles (sc-108084) according to manufacturer's instructions (Santa Cruz Biotechnology). TRPV1-knockdown efficiency was evaluated by immunoblot analysis and Ca^{2+} imaging after 7–10 d of selection with puromycin (2 μg/ml).

Single-cell Ca^{2+} imaging. Naive $CD4^+$ T cells isolated from the spleen of wild-type, *Trpv1*$^{-/-}$ or *Trpv1*-TG mice were loaded for 30 min at 22–25 °C with 1 μM Fura-2 AM (Molecular Probes) in culture medium (at a density of 1×10^6 cells per ml), then were washed and attached for 15 min to poly-D-lysine–coated coverslips. For measurement of $[Ca^{2+}]_i$, coverslips were mounted on an RC-20 closed-bath flow chamber (Warner Instrument) and were analyzed on an Olympus IX51 epifluorescence microscope with Slidebook imaging software (Intelligent Imaging Innovations) as described[44]. Store-operated Ca^{2+} was measured after passive depletion of intracellular stores with 1 μM thapsigargin. For stimulation of the TCR, cells were first pretreated with 5 μg/ml of biotinylated anti-CD3 (145-2C11; eBioscience) and TCRs were crosslinked with 10 μg/ml of ImmunoPure streptavidin (Pierce). For measurement of TRPV1 activity, cells were perfused with Ringer's solution containing 1 or 10 μM capsaicin. Fura-2 emission was detected at 510 nm with excitation at 340 and 380 nm, and the ratio of Fura-2 emission at 340 nm to that at 380 nm (340/380) was acquired at intervals of 5 s after subtraction of background. For each experiment, 50–100 individual cells were analyzed with OriginPro analysis software (Originlab). For measurement of $[Ca^{2+}]_i$ in Jurkat T cells, the Fura-2 fluorescence ratios were collected on a Nikon microscope stage equipped with a 40× Nikon UV-Fluor objective and an intensified CCD camera (ICCD200). The fluorescence signals emitted from the cells were monitored continuously at intervals of 5 s with the MetaFluor Imaging System (Universal Imaging) and were recorded for later analysis. Peak or sustained Ca^{2+} ratios were calculated as the maximal Ca^{2+} that accumulated in the cell after subtraction of baseline amounts (before the addition of Ca^{2+}-containing Ringer's solution), after reintroduction of Ca^{2+}-containing Ringer's solution. All experiments were performed at room temperature (22–25 °C).

Measurement of Ca^{2+} flux by flow cytometry. $CD4^+$ T cells were isolated from the spleen of wild-type, *Trpv1*$^{-/-}$, *Trpv1*-TG or *Trpv3*$^{-/-}$ mice and $[Ca^{2+}]_i$ was measured as described[45,46]. Cells were suspended at a density of 2.5×10^6 cells per ml in 2% FBS in PBS and were prelabeled for 10 min at 37 °C with 40 nM CFSE (carboxyfluorescein diacetate succinimidyl ester; Invitrogen) or were mock-treated and mixed in equal proportions (for example, wild-type cells (CFSE) plus *Trpv1*$^{-/-}$ cells (mock)). In some experiments, the CFSE- and mock-treated pairs were reversed to ensure that the CFSE staining did not alter the results. Cells were washed, then were resuspended at a density of 5×10^6 cells per ml in2% FBS in PBS and were incubated for 30 min at 37 °C in 5% CO_2 with 2 μM Indo-1 AM (Molecular Probes). Cells were then washed, stained with allophycocyanin–anti-CD4 (GK1.5; eBioscience) and resuspended a density of 1×10^6 cells per ml in complete RPMI medium. Finally, cells were transferred to calcium-free medium (Ca^{2+}- and Mg^{2+}-free Hank's balanced-salt solution supplemented with 2% FCS and 1 mM EGTA) just before the beginning of the acquisition. Cells were preincubated or not for 5 min at 37 °C with various concentrations of TRPV1 antagonists (BCTC or I-RTX) or with vehicle (0.1% DMSO) and were stimulated at 37 °C with 1 or 10 μM capsaicin, 10 μg/ml anti-CD3 and 1 μg/ml anti-CD28 (antibodies identified above) or, alternatively, with 500 nM of ionomycin or 1 μM thapsigargin. Various concentrations of $CaCl_2$ were added during the analysis on a BD LSR II flow cytometer. Data are presented as the ratio of Indo-1 fluorescence violet (405 nm) to blue (510 nm) and were calculated on gated $CD4^+$ cells with FlowJo software (TreeStar).

Flow cytometry. For staining of surface markers, mouse and human $CD4^+$ T cells were stained for 30 min at 4 °C with allophycocyanin-conjugated antibody to mouse CD4 (GK1.5), Alexa Fluor 488–conjugated antibody to mouse CD25 (3C7), phycoerythrin-conjugated antibody to mouse CD45RB (C363.16A) and peridinin chlorophyll protein–cyanine 5.5–conjugated antibody to mouse TCRβ (H57-597; all from eBioscience) or with peridinin chlorophyll protein–cyanine 5.5–conjugated antibody to human CD4 (RPA-T4), phycoerythrin-conjugated antibody to human CD25 (BC96) and fluorescein isothiocyanate–conjugated antibody to human HLA-DR (L243; all from eBioscience), respectively. For intracellular staining, cells were fixed for 10 min at room temperature in 2% paraformaldehyde in PBS, then were centrifuged and permeabilized for 15 min at 4 °C in 0.2% Triton X-100 (staining of TRPV1) or in ice-cold 100% methanol (staining of phosphorylated PLC-γ1). For staining of TRPV1, cells were then washed, nonspecific binding was blocked for 30 min at 4 °C with 5% BSA in PBS, and cells were preincubated or not for 2 h at room temperature with tenfold excess of specific blocking peptide, then were stained for 1 h at 4 °C with goat anti-TRPV1 (sc-12498) or normal goat IgG (sc-2028) as a control. For intracellular staining of phosphorylated PLC-γ1, cells were incubated with monoclonal anti-mouse CD16/CD32 (Fc Block; 2.4 G2; BD Biosciences) and were stained for 30 min at 4 °C with antibody to phosphorylated PLC-γ1 (2821; Cell Signaling Technology). All primary antibodies were used at a dilution of 1:100 unless indicated otherwise. Cells were then washed and incubated for 30 min at 4 °C with allophycocyanin-conjugated antibody to mouse CD4 (GK1.5; eBioscience) and peridinin chlorophyll protein–cyanine 5.5–conjugated antibody to mouse TCRβ (H57-597; eBioscience) together with the secondary antibodies (both at dilution of 1:500) Alexa FLuor 488–conjugated anti-rabbit (for phosphorylated PLC-γ1; A11008; Invitrogen) or with Alexa FLuor 488–conjugated anti-goat (TRPV1 staining; A11078; Invitrogen). Cells were finally washed and analyzed on a BD FACSCalibur or Accuri C6 flow cytometer. The data were analyzed with FlowJo software (TreeStar).

Biotinylation of cell surface proteins. Surface proteins on Jurkat T cells were biotinylated and immunoprecipitated with a cell surface protein–isolation kit from Pierce (89881) according to the manufacturer's instructions (Thermo Scientific). 25×10^6 Jurkat T cells expressing green fluorescent protein (control) or Jurkat T cells in which TRPV1 was knocked down were biotinylated for 30 min at 4 °C under gentle agitation with a solution of EZ-Link Sulfo-NHS-SS-Biotin in PBS (0.25 mg/ml). After reactions were quenched and cells were lysed, the biotinylated proteins were isolated by NeutrAvidin agarose beads (Pierce) and were eluted from the beads by incubation for 60 min at room temperature in SDS-PAGE sample buffer (62.5 mM Tris-HCl, pH 6.8, 1% SDS, 10% glycerol and 50 mM DTT). A sample of the initial cell lysates was retained for analysis of total proteins. Proteins were resolved by SDS-PAGE as described above (immunoblot analysis).

CFSE proliferation assay. Isolated splenic $CD4^+$ T cells were suspended in a solution of 2% FBS in PBS at a density of 10×10^6 cells/ml. A 100 μM working dilution was prepared in a solution of 2% FBS in PBS from the CFSE stock solution (5 mM in DMSO). CFSE was added to the cells at a final concentration of 1 μM and the cells were incubated at 37 °C for 7 min. Incorporation of CFSE into cell membranes was stopped by the addition of five volumes of ice-cold RPMI medium supplemented with 30% FBS. Excess CFSE was removed by three successive washes in medium. Dilution of CFSE in dividing cells was monitored at 72 h after stimulation with 10 μg/ml anti-CD3 and 1 μg/ml anti-CD28 (antibodies identified above) or with PMA (25 ng/ml) plus ionomycin (500 nM) and was assessed by flow cytometry on gated $CD4^+$ T cells.

Immunofluorescent staining and confocal microscopy. Splenic $CD4^+$ T cells were isolated as described above and were 'cytocentrifuged' (Cytospin 2; Shandon) for 3 min at 500 r.p.m. onto microscope slides. Alternatively, Chinese hamster ovary cells, either control or overexpressing rat TRPV1, were grown for 1–2 d on collagen type 1–coated coverslips (BD Biosciences) in complete DMEM-F12 supplemented with geneticin (1.2 mg/ml) (cells overexpressing rat TRPV1) or not (control cells). The air-dried cytospin preparations or the coverslips were fixed for 10 min at room temperature in a solution of 4% paraformaldehyde in PBS and were permeabilized for 15 min at 4 °C in 0.2% Triton X-100. Cells were then washed, nonspecific binding was blocked for 30 min at 4 °C with 5% BSA and 0.2% Triton X-100 in PBS and cells were stained for 1 h at 4 °C with goat anti-TRPV1 (sc-12498; Santa Cruz Biotechnology) or with normal goat IgG (sc-2028; Santa Cruz Biotechnology). Cells were washed

© 2014 Nature America, Inc. All rights reserved.

and then were incubated for 30 min at 4 °C with Alexa Fluor 488–conjugated anti-CD4 (GK1.5; eBioscience) and the secondary antibody Alexa Fluor 546–conjugated anti-goat (A21085; Invitrogen). For TCR-clustering experiments, splenic $CD4^+$ T cells were pretreated or not for 1 h at 37 °C with 10 μM PP2 before being incubated for 30 min on ice with a hamster anti-CD3 (20 μg/ml soluble; 145-2c11; BioXcell). The cells were washed, stained for 30 min on ice in the dark with a secondary antibody Alexa Fluor 488–conjugated anti-hamster (A21110; Invitrogen), and were left unstimulated or stimulated for 5 min at 37 °C with anti-CD3 as described above. Cells were stained for TRPV1 as described above, or for 1 h at 4 °C with rabbit antibody to Lck (sc-13; Santa Cruz Biotechnology) and for 30 min at 4 °C with the secondary antibody Alexa Fluor 647–anti-rabbit (A21244; Invitrogen). All primary and secondary antibodies were used at a dilution of 1:100 unless indicated otherwise. One cytospin preparation served as a negative control staining with the control antibody IgG or the secondary antibodies only. Cells were finally stained for 10 min at room temperature with Hoechst 33342 (50 ng/ml; Invitrogen) and rinsed with deionized water and slides were mounted in ProLong Gold antifade reagent (Invitrogen). The fluorescence images were acquired using a 100× oil-immersion objective on a confocal laser-scanning microscope (Olympus IX81) with Fluoview software. Colocalization was assessed with Velocity software.

Electrophysiological assay. Whole-cell patch-clamp recording and analysis were carried out on an Axopatch 200B amplifier with Digidata1322A interface and pClamp9 software (Axon Instruments). Patch electrodes were pulled from thin-walled borosilicate glass (World Precision Instruments) on a horizontal micropipette puller (Sutter Instruments). Electrodes had a resistance of 8-20 MΩ when filled with intracellular solution. Analog capacity compensation and series resistance compensation were used during whole-cell recordings. For single pulse recordings, spleen $CD4^+$ T cells were held at −85 mV and 16 μM capsaicin was introduced via a gravity-fed perfusion system into the recording chamber with a TC344B heater controller and an SH-27B inline heater (Warner instruments). For experiments performed in the presence of SB366791, cells were pretreated for 30 min in external solution containing 1 μM SB366791, and currents were then recorded in the presence of both capsaicin (16 μM) and SB366791 (1 μM). For TCR stimulation, cells were first pretreated for 20 min at 4 °C with biotinylated anti-CD3 (20 μg/ml; 145-2C11; eBioscience), and then they were activated by the addition of streptavidin (10 μg/ml) in the external solution and were held at −85 mV. Data were sampled at 10 kHz and filtered at 5 kHz, and whole-cell recordings were performed at 35 °C. The extracellular solution contained 144 mM NaCl, 5 mM KCl, 2 mM MgCl2, 1 mM CaCl2, 10 mM glucose and 10 mM HEPES and was adjusted to a pH of 7.4 with NaOH. The intracellular solution used in the pipettes contained 126 mM K-gluconate, 10 mM KCl, 5 mM EGTA, 4 mM MgATP and 10 mM HEPES and was adjusted to a pH of 7.4 with KOH. For analysis of current-voltage relationships, the external solution contained 140 mM NaCl, 5 mM KCl, 2 mM $MgCl_2$, 5 mM EGTA, 10 mM HEPES and 10 mM glucose and was adjusted to a pH of 7.2 with NaOH. The internal solution contained 136 mM CsCl, 5 mM EGTA, 10 mM HEPES and 4 mM MgATP and was adjusted to a pH of 7.4 with NaOH. Liquid junction potential was calculated at +15 mV and was corrected offline.

Electrophoretic mobility-shift assay, immunoprecipitation and immunoblot analysis. For assessment of translocation of NF-κB and NFAT-1 to the nucleus in wild-type and *Trpv1*$^{-/-}$ spleen $CD4^+$ T cells, cytoplasmic cell extracts were made by lysis via incubation for 5 min on ice in hypotonic lysis buffer A (10 mM HEPES, pH 7.9, 10 mM KCl, 0.1 mM EDTA and complete protease inhibitors (Roche)). After collection of the cytoplasmic extracts, cell pellets were lysed for 5 min on ice in nuclear extract buffer B (20 mM HEPES, pH 7.9, 420 mM NaCl, 1 mM EDTA and protease inhibitors). Translocation of activated NF-κB into the nucleus was measured by electrophoretic mobility-shift assay with consensus NF-κB oligonucleotides (Santa Cruz Biotechnologies) as described[42]. Translocation of NFAT-1 was analyzed in the nuclear fractions by immunoblot with mouse monoclonal anti-NFAT-1 (ab2722; Abcam). The phosphorylation of Zap70, Lat, Erk1/2, p38 and Jnk was assessed in the cytosolic fraction with antibodies specific for the phosphorylated and total forms of these proteins (antibodies identified above). The protein concentration was determined with a protein-quantification kit (Bio-Rad). Protein samples (10 μg/lane) were separated by SDS PAGE (4–12% acrylamide NuPAGE Novex bis-Tris precast gels; Life Technologies) and then were transferred to PVDF membranes (Millipore). Nonspecific binding in the blots was blocked by incubation for 45 min at room temperature in 5% BSA and 0.3% Tween-20 in PBS, and blots were incubated overnight at 4 °C with primary antibodies (identified above; all at a dilution of 1:1,000). The blots were washed and then were incubated for 45 min at room temperature with their corresponding horseradish peroxidase–conjugated secondary antibody (705-035-003, 115-035-174 and 711-065-152; Jackson ImmunoResearch Laboratories; each at a dilution of 1:5,000 to 1:10,000) and were developed in ECL solution (Pierce). Image J software was used for quantification of immunoblot analysis results by band densitometry. For measurement of TRPV1 expression by immunoblot analysis, resting mouse and human primary $CD4^+$ T cells, Jurkat T cells, and control or rat TRPV1–overexpressing Chinese hamster ovary cells, were lysed with RIPA buffer (Teknova) supplemented with protease inhibitors (Roche), followed by immunoblot analysis as described above with anti-TRPV1 (sc-12498 (Santa Cruz) at a dilution of 1:1,000, or ACC-030 (Alomone) at a dilution of 1:200). For analysis of the tyrosine phosphorylation of TRPV1, wild-type and *Lck*$^{-/-}$ Jurkat T cells were left resting or were stimulated with 2.5 μg/ml anti-human CD3 plus 1 μg/ml anti-human CD28 (antibodies identified above) and then were lysed with RIPA buffer supplemented with protease inhibitors (Roche), then proteins were immunoprecipitated from cleared lysates by incubation overnight at 4 °C with goat anti-TRPV1 (sc-12498; Santa Cruz Biotechnology) coupled to protein A magnetic beads (New England Biolabs). Normal goat IgG was used as negative control (sc-2028; Santa Cruz Biotechnology). Then the immunoprecipitates were washed three times with lysis buffer and separated by SDS-PAGE. Blots were probed with antibodies to phosphorylated tyrosine, anti-TRPV1 and anti-Lck as described above (antibodies identified above).

***Il10*$^{-/-}$ model of colitis.** 8- to 10-week-old sex- and age-matched *Il10*$^{-/-}$ or *Il10*$^{-/-}$*Trpv1*$^{-/-}$ mice were randomly assigned to experimental groups. To overcome the variability in severity and onset of the disease in this model, colitis was induced by treatment with the nonsteroidal anti-inflammatory drug piroxicam[26] (Sigma). Mice were fed normal chow for 14 consecutive days, without mixture or mixed with piroxicam (50 mg per 250 g chow for the first week and 70 mg per 250 g chow for the second week). In some experiments, *Il10*$^{-/-}$ mice were treated daily with SB366791 (3 mg per kg body weight; given intraperitoneally) or with vehicle (10% DMSO and 90% saline) starting 3 d before and daily during the 14 d of the colitis induction by piroxicam. Wasting disease in the groups was monitored periodically and mice were killed at day 30 for analysis.

T cell–adoptive transfer model of colitis. Splenic naive $CD4^+$ T cells isolated from wild-type, *Trpv1*$^{-/-}$ or *Trpv1*-TG donor mice were adoptively transferred into *Rag1*$^{-/-}$ or *Rag1*$^{-/-}$*Trpv1*$^{-/-}$ recipients as described[47,48]. Samples were enriched for $CD4^+$ T cells by immunomagnetic negative selection, then cells were stained with allophycocyanin–anti-CD4 Alexa Fluor 488–anti-CD25 and phycoerythrin–anti-CD45RB (antibodies identified above) and were sorted into populations of naive $CD4^+CD45RB^{hi}CD25^-$ cells and regulatory $CD4^+CD45RB^{lo}CD25^+$ cells (usual purity, >98%) with a BD FACSAria II flow cytometer. 8- to 10-week-old sex- and age-matched *Rag1*$^{-/-}$ or *Rag1*$^{-/-}$ *Trpv1*$^{-/-}$ recipients were reconstituted by intraperitoneal injection of 3×10^5 naive $CD4^+$ T cells from wild-type, *Trpv1*$^{-/-}$ or *Trpv1*-TG sex-matched donor mice. For cotransfer experiments, 1.5×10^5 T_{reg} cells from wild-type mice were injected together with the naive $CD4^+$ T cells. After reconstitution, mice were monitored weekly for signs of intestinal inflammation, such as weight loss and diarrhea. The disease activity index (the combined score of weight loss and bleeding) was determined as described[47,48]. Diseased mice were killed for analysis.

Isolation of lamina propria lymphocytes. Lamina propria lymphocytes were isolated as described[47]. Colons were washed with PBS and cut into small pieces (~1–2 mm in width). Tissue pieces were digested twice for 30 min at 37 °C, under rotation, with PBS containing 0.5 mg/ml of collagenase IV and 0.5 mg/ml of DNase I (both from Sigma). Cell suspensions containing lamina

© 2014 Nature America, Inc. All rights reserved.

doi:10.1038/ni.3009

propria lymphocytes were collected through a 40-μm cell strainer. Finally, the lymphocytes were isolated by centrifugation at 1,000*g* (without braking) for 20 min at 20 °C with a 40/80 gradient of Percoll (GE Healthcare) (usual $CD4^+$ T cell purity, >80%).

Colonic explants. Colonic longitudinal sections (~3–4 mm in width) were weighed and then were washed in RPMI medium 1640 containing 100 μg/ml streptomycin and 100 U/ml penicillin. The colonic explants were cultured for 24 h at 37 °C and 5% CO_2 in complete RPMI-1640 medium. Culture supernatants were then collected and cytokines were measured (by ELISA).

Histological analysis. Entire colons were excised, opened longitudinally, rolled onto a wooden dowel and fixed with 10% buffered formalin. Paraffin sections (5 μm in thickness) were stained with hematoxylin and eosin. Colonic epithelial damage was assigned scores (by researchers 'blinded' to sample identity) as follows: 0, normal; 1, hyperproliferation, irregular crypts and goblet cell loss; 2, mild to moderate crypt loss (10–50%); 3, severe crypt loss (50–90%); 4, complete crypt loss with surface epithelium intact; 5, small- to medium-sized ulcer (<10 crypt widths); and 6, large ulcer (>10 crypt widths). Infiltration with inflammatory cells was assigned scores separately for the mucosa (0, normal; 1, mild; 2, modest; and 3, severe), submucosa (0, normal; 1, mild to modest; and 2, severe), and muscle plus serosa (0, normal; 1, moderate to severe). Scores for epithelial damage and inflammatory cell infiltration were added, which resulted in a total colitis scoring range of 0–12.

Statistical analysis. The statistical significance between two groups was determined with an unpaired Student's *t*-test with two-tailed *P* values. The statistical significance of differences between more than two groups was determined by one-way ANOVA with a *post-hoc* Dunnett's or Bonferroni test. For time-course experiments *in vivo*, two-way ANOVA with a *post-hoc* Bonferroni test was used. All statistical results were analyzed with PRISM software (GraphPad).

41. Moqrich, A. *et al.* Impaired thermosensation in mice lacking TRPV3, a heat and camphor sensor in the skin. *Science* **307**, 1468–1472 (2005).
42. González-Navajas, J.M. *et al.* Interleukin 1 receptor signaling regulates DUBA expression and facilitates Toll-like receptor 9-driven antiinflammatory cytokine production. *J. Exp. Med.* **207**, 2799–2807 (2010).
43. Franco, A., Shimizu, C., Tremoulet, A.H. & Burns, J.C. Memory T cells and characterization of peripheral T cell clones in acute Kawasaki disease. *Autoimmunity* **43**, 317–324 (2010).
44. Srikanth, S., Jung, H.J., Ribalet, B. & Gwack, Y. The intracellular loop of Orai1 plays a central role in fast inactivation of Ca^{2+} release-activated Ca^{2+} channels. *J. Biol. Chem.* **285**, 5066–5075 (2010).
45. Fu, G. & Gascoigne, N.R. Multiplexed labeling of samples with cell tracking dyes facilitates rapid and accurate internally controlled calcium flux measurement by flow cytometry. *J. Immunol. Methods* **350**, 194–199 (2009).
46. Fu, G. *et al.* Themis controls thymocyte selection through regulation of T cell antigen receptor-mediated signaling. *Nat. Immunol.* **10**, 848–856 (2009).
47. González-Navajas, J.M. *et al.* TLR4 signaling in effector $CD4^+$ T cells regulates TCR activation and experimental colitis in mice. *J. Clin. Invest.* **120**, 570–581 (2010).
48. Li, X. *et al.* Divergent requirement for Gαs and cAMP in the differentiation and inflammatory profile of distinct mouse Th subsets. *J. Clin. Invest.* **122**, 963–973 (2012).

© 2014 Nature America, Inc. All rights reserved.